University of Wisconsin Milwaukee
UWM Digital Commons

Theses and Dissertations

May 2017

Ground Fault Location of Cable Using Wavelet in DC Microgrid

Junyang Yu
University of Wisconsin-Milwaukee

Follow this and additional works at: https://dc.uwm.edu/etd

 Part of the Electrical and Electronics Commons

Recommended Citation
Yu, Junyang, "Ground Fault Location of Cable Using Wavelet in DC Microgrid" (2017). *Theses and Dissertations*. 1561.
https://dc.uwm.edu/etd/1561

This Thesis is brought to you for free and open access by UWM Digital Commons. It has been accepted for inclusion in Theses and Dissertations by an authorized administrator of UWM Digital Commons. For more information, please contact open-access@uwm.edu.

GROUND FAULT LOCATION OF CABLE USING WAVELET IN DC MICROGRID

by

Junyang Yu

A Thesis Submitted in

Partial Fulfillment of the

Requirements for the Degree of

Master of Science

in Engineering

at

The University of Wisconsin-Milwaukee

May 2017

ABSTRACT

GROUND FAULT LOCATION OF CABLE USING WAVELET
IN DC MICROGRID

by

Junyang Yu

The University of Wisconsin-Milwaukee, 2017
Under the Supervision of Professor Robert M. Cuzner

As the proliferations of distributed generation and power electronic equipment in power systems, more and more researchers put focus on the DC microgrid. This study is based on cables in DC community microgrid. Single ground fault is considered in the cables connected hub garage and participating garages. With long length compared to other cables in the system, it is necessary to study the method to locate the ground fault when the fault happen in the buried cables.

Two approaches are studied. The traveling wave method is applied for analysis of transient process when the fault happens while the stable parameter analysis method used for the stable process after the fault already happened.

The cable model is defined using precise distributed element concept and packaged as a PLECS model. The simulation is based on the DC microgrid model in the Simulink environment with PLECS blocks.

The wavelet packet decomposition is applied in the processing of signal processing procedure. The wavelet packet helps to extract the key signal and eliminate the interference in both methods respectively. The results are analyzed to show the effectiveness of location methods and wavelet packet.

© Copyright by Junyang Yu, 2017
All Rights Reserved

TABLE OF CONTENTS

LIST OF FIGURES

LIST OF TABLES

ACKNOWLEDGEMENTS

It is absolutely an unforgettable experience in University of Wisconsin Milwaukee during this time.

Thanks for my instructor, Professor Robert M Cuzner, who is always helpful and patient. I am touched by his infinite energy in research and teaching. And I think I learnt more from the spirit of research rather than the knowledge itself from my professor. I am always looking forward to collaborating with Dr. Cuzner in the future.

I would also thank for my friend Mengyuan and Haibo, who is from the same university in China and live in the same apartment with me. Jiayan and Mengfan, who also come from Chongqing University, also helped me a lot. I had some fantastic time with Yihui, and other friends from NCEPU, too. I feel warm as back in the campus in China because of you.

This is the first time I've been abroad for such a long time. I would specially appreciate everything given by my foreign friends: Christina and Jared, along with Grace, Hannah, Jaiwon, Rebecca, Saia and Sara. I may not list all of them here, but the friendship created among us is always the reason I feel the beauty of life.

My family supports me before and during the whole time. I cannot reach this goal without their selfless help from every aspect.

I am glad to have this epic journey in Milwaukee with full happiness. Thank you all.

Chapter 1 Introduction

In this chapter, the background, research status and general approach are presented. The research in general of this thesis are presented in the last paragraphs.

1.1 Background

1.1.1 DC Microgrid

New era comes with new energy sources. Solar, wind, tide and other new energy sources emerged as the word “renewable energy” become popular. As the lack of regular energy source and problem of environment pollution get severe, the clean and renewable energy source will take more weight in total power generation. With the maturity of distributed energy technology, and the high growth of generation capacity, supply system for residential users are developed towards a multiple type based and sustainable goal gradually. Finally, the new term “microgrid” came out, representing the core part of smart grid [1]. Compared to classic utility grid, microgrid can operate with or without connect to the utility grid, providing a low-cost, distributed energy source friendly, and quick response power supplier while enhance the reliability in general [2].

Innovative types of distributed generation system like Photovoltaic architecture integrated system, wind turbine for buildings and family-use fuel cell generation system have emerged. For normal early implemented AC microgrid, the DC generation component will increase the losses through the AC distribution network, especially in the converter / inverter components. The DC microgrid is being promoted as people find its advantages step by step on the development of electrical engineering nowadays: The huge capacity high voltage direct current (HVDC) is widely used in various countries for main power transmission, and the efficiency of DC/DC converter has been

increased to a satisfactory level. Another reason to apply the DC directly supply, is that the number and type of devices that using DC source is increasing fast. DC motor and smart devices which take heavier role in our life will perform better if there is DC source connected to the community power network [3]. In general, it is reasonable to apply the low voltage as well in the community grid nowadays as it will be economic and saves more energy.

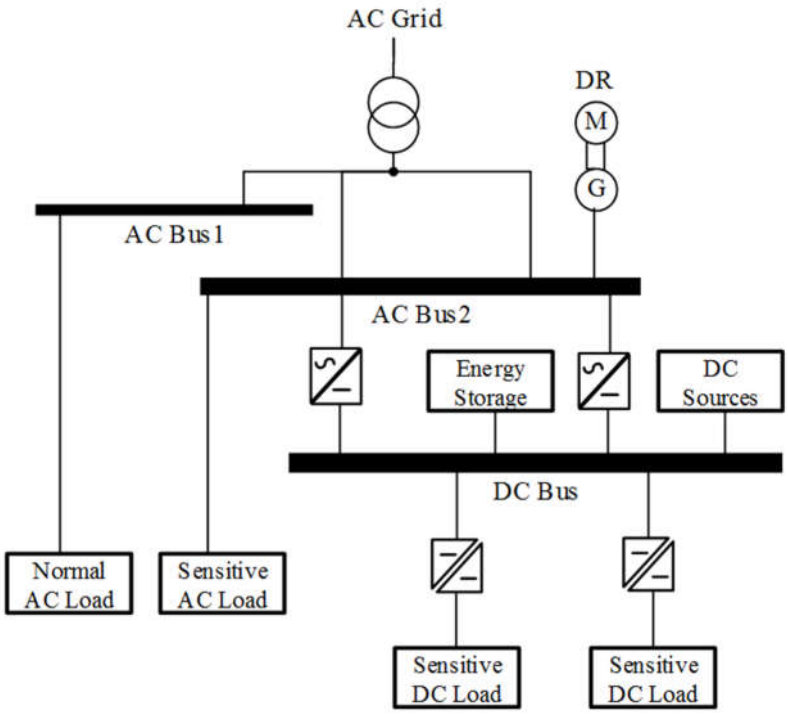

Figure 1-1 Common Structure of DC Microgrid

Figure 1-1 shows a typical DC microgrid structure with AC-DC mixed sources and loads where called hybrid microgrid in [4]. From the source aspect, the DC sources including like wind generator and PV panels are providing the DC power with the energy storage like batteries. In the other hand the traditional AC power is providing the DC load through the high efficiency converters. From the load aspect, both AC and DC devices exist, which means these loads can both be directed feed by its power sources and the AC-DC mixed source structure is needed.

1.1.2 Power Cables and its Ground Fault

For power transmission, overhead line and underground cables are usually choices. As the urbanization level increase, new challenges emerge as the density of population, larger malls and intense entertainment region, and more vehicles with roads. The room for power distribution is decreasing while safety standards becoming stricter. The transmission line will occupy overmuch in aboveground space, and be dangerous when it is damaged caused by traffic accidents and bad weather as its core is bare to the environment. As another method, the power cables have obvious advantages over the transmission lines: it takes less space not influencing the normal human activity in the ground, consists multi cables in the same cable tunnel, not sensitive to the climate and weather and runs with more reliability.

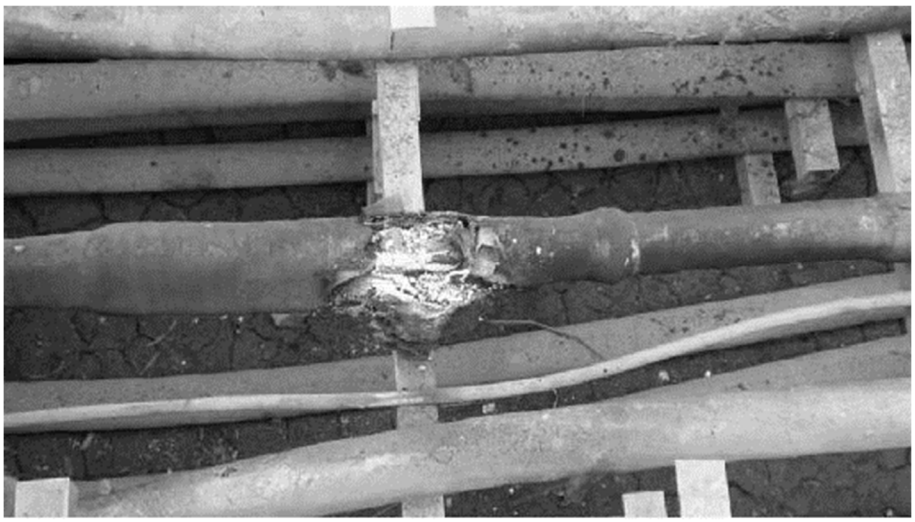

Figure 1-2 Corrupt Cable that Cause Ground Fault

But other threats towards power cables remain. Due to long time burying underground, it becomes relatively vulnerable. The outside force will lead the power cable into damage. The power cables cannot be bare to the ground, the insulation layer help protect its current and voltage from outside world. But when the insulation defect exists which is from the long time affection of moisture, acid or base component in soil, even animals bite, the core of cable will develop gradually to be

exposed to the outside or other cable, and finally threaten the normal operation of power grid and the safety of human and devices on the ground. Figure 1-2 shows such a situation that the protect and insulation layers are damaged and the core of cable can be directly contacted by the outside. Several faults may happen in the power grid caused by the power cables. They can be classified from different aspects.

Table 1-1 Classification of Fault Types

Classification Basis	**Fault Types**
Location	Cable Fault, Cable Joint Fault
Fault Appearance	Open Fault, Closed Fault
Fault Time	Operation Fault, Experiment Fault
Ground	Line-Line Fault, Single Ground Fault, Multi-ground Fault, Open Circuit Fault
Fault Impedance	Short Fault, Low Impedance Fault, High Impendence Fault, Open Circuit Fault, Arc-over Fault

Table 1-1 shows the different cable faults classified by the basis. What is important in this research is that, the single ground fault is the main target, and its fault impedance will look like a low impedance, even short fault. The cable itself is assumed as the fault where it happens, since the joint fault will have different appearance from the outside monitoring. As it is a single ground fault, the fault will appear as an open fault since it's influencing the outside by soil.

1.2 Research Status

The prerequisite to ensure the power transmission system using power cables under the safe operation is proper monitor and detection of every component. The detecting system about cables is one of key elements of the overall power system monitoring.

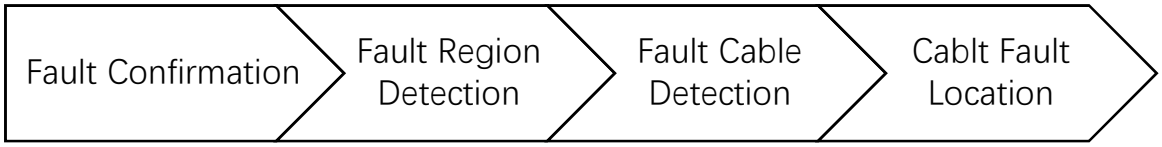

Figure 1-3 The Procedure of Locating a Fault in Cable

It is necessary to detect the fault happens in the cables as well as locate the fault point. In general, the location of fault in cable is considered as subsequent procedure after a series previous detection as it is shown in Figure 1-3. The protection system will decide whether there is a fault and then trying to locate from a large scale area all the way to the cable fault location if system decide there is fault in the cable. It should be noted in reality the location of cable may not be triggered by this procedure, which means the fault location can be processed as an individual part.

Lots of researches are focusing on this area since the cable were widely used in the power transmission. In the old time, to enable the detection of cables must cut the power between the cable which will cause region breakout. It not only creates huge economy losses, but also take considerable human resources and time because the old method need complicated operation with relative low precision.

Nowadays scientists are developing new ways to locate the fault in cables. Online location can be achieved in some ways like [5] while the offline location is easier to apply with higher precision than before like [6]. The admissive detection method for fault location in DC cables contains stable parameter shown in papers like [7] and [8] and traveling wave analysis shown in [9]. But due to the limitation of available use space and accuracy, only using these methods did not receive

satisfied result. Later, signal processing and smart intelligence technology like [10],[11], even with multiply domain analysis [12] were introduced in the cable fault and location diagnose, which successfully improve the performance of both methods.

No matter using traveling wave or impedance analysis, the data processing part has developed several techniques. Wavelet are used into cables for several years. The main use for applying the wavelet is trying to extract the characteristic signal from the original signal in sensors. With different wavelet transform application and extraction strategy, scientists have developed multiple methods to recognize the type and location of cable. As the wavelet can be used in the denoising area, it also can be used in this way for both de-nosing and recognition purposes. Neutral network was introduced later with combination of wavelet transform. The neural network can be used as a smart tool to diagnose the fault by self-learning. As the cloud data and big data concept developing, like Distribution Fault Anticipation in [13], with distributed and cloud computing's help, the neural network can be widely applied when the number of DC microgrid grows. Other theories, such as mathematical morphology [14] and chaos theory [15]are researched to be collaborated with cable fault detection and location. As a comprehensive method, in the last, people are trying to build the smart diagnosis system integrated with some methods as well as other fault detection system in the DC microgrid like in this research [16]. This will use the cable signal as well as its front-end and back-end even the bus signals to analyze the fault information.

1.3 General Approach

As it is mentioned above, traveling wave and impedance analysis are popular methods. These two methods along with other available location methods are introduced below.

1.3.1 Traveling Wave Method

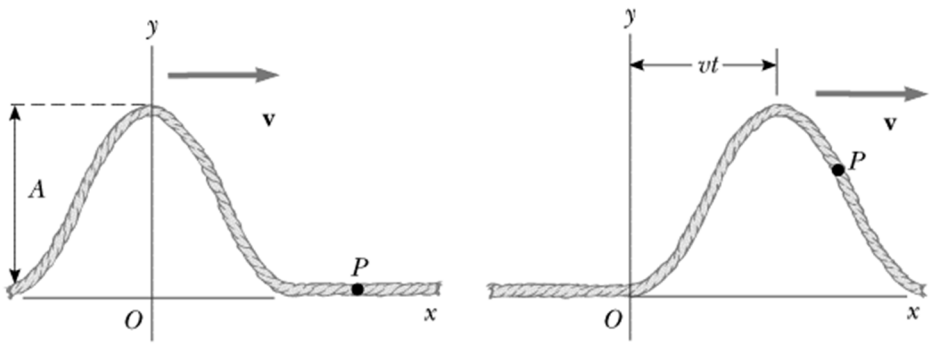

Figure 1-4 Concept of Traveling Wave

In relative long cables, as the distributed elements existed everywhere along the cable. The current and voltage will spend a time to reach the destination. Figure 1-4 shows, if the input signal is a pulse, the current and voltage will look like a move in a rope moving forward if we see the whole length cable in the same time. Traveling wave also have a speed as most waves in the physics world and it is decided by the cable electric parameters.

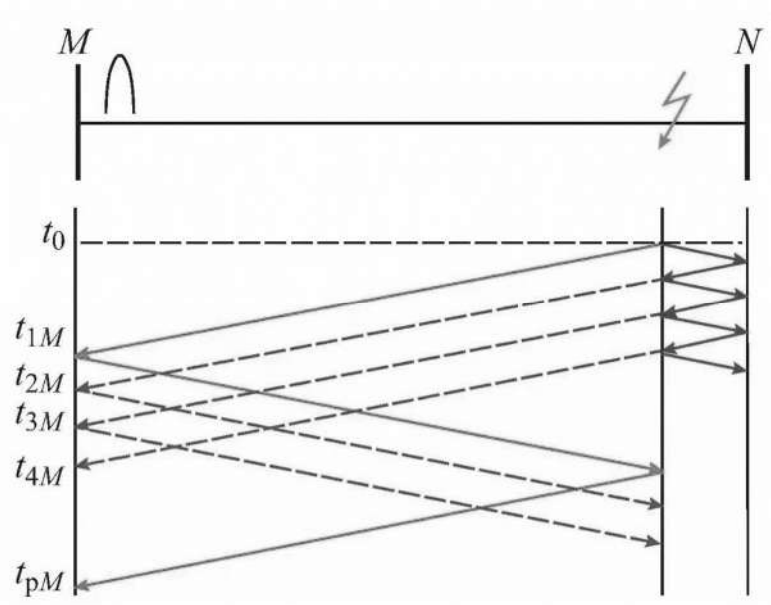

Figure 1-5 The Reflection of Traveling Wave when Fault Happens in Cable

The damaged point in the cable, having the different impedance characteristics, will lead to the traveling wave reflection. In Figure 1-5 we can see the what the traveling wave will travel after

the fault happens. Divided by the fault point, both side will generate the new traveling wave according to the ground features. It should be noted that the traveling wave will bounce multiple times, which will transit to stable situation in the final. This feature gives us a chance to measure the distance of fault in that transient process using the initial traveling wave, but also tells us the time is limited as it will become a stable situation that becomes harder for extract the characteristics signals. This is described as the transient analysis in the article, which is the main part in the Chapter 4.

There are some applications using an exterior signal injection for traveling wave method. The measurement is mostly focused on the current since the voltage are harder to fetch and current signal normally have a higher amplitude. Surge current is widely used method that can be applied in most situations. It need a high current generator and will influence the normal operation of the cable. The high amplitude itself can damage the other position of the cable as well as the safety of location process. Secondary breakdown method is used for some high voltage cables, where signals are compared with one low current signal sent accompanying with a high surge current and one just normal low current signal. The signal with the surge will travel all the way to the end of cable due to the link on arc generated by the surge. And the other signal will remain open at the fault position. Then calculation is drawn to get the fault distance. Some online approaches are developed recently in [17] and [18], but still need to be proven in more situations.

1.3.2 Stable Parameter Analysis Method

The second way, is the stable parameter analysis, or called dc impedance measurement method for most application. A classic approach using the impedance analysis is electrical bridge method which is provided for a long time [19]. The basic of the theory is easy: there must be a connection between the fault current, the location of fault, voltage and so on since the cable is consider as

infinite parts of electrical components. A certain function can be derived showing the certain relationship of fault current (ground current) and fault location with other parameters represented for the situation.

Most methods developed for the impedance analysis is based on mathematic aspect. Model analysis, first-order equation, second-order equation, differential equation and iteration method can be used to establish the relation. Neural network is used to create black box connected between the input signal and location result, which is actually similar method.

Other methods can be utilized to help locate the fault too. As one of them, sound-magnetic detection is a possible way to detect the location of fault: After injecting a high amplitude surge current, the fault point will generate an arc with a loud and sharp sound and an obvious magnetic field. By high sensitive sound and magnetic field sensor, the fault can be located within a certain range. Even injecting sound signals can be achieved in certain cases as the sound will generate a various magnetic field appearance. Using electromagnetic filed or ultrasonic related detection [20] can be also useful in some situations.

Besides the traveling wave and impedance analysis, whether need an exterior signal can also lead to different research and implement realizations. Using exterior signal, like using current injection technic in [21], often results in the high-definition data related to the fault since the signal usually contains high amplitude impulse which exists in every frequency bands. But the position to inject the signal is hard to apply especially it is required to be online monitoring and detected without shut the power grid down. The equipment itself also can be a burden to some users who have limited budget.

As the background of this DC community microgrid, using original fault signals may be more reasonable compared to using an exterior signal generator. In that way, no more devices would be

used and trying to detect the location should be implemented with the signal that already exists in the system.

1.4 Thesis Structure

This article is written with parts below:

1 First introduce the background of this research and the research status. The basic concepts of two major fault location methods are described too.

2 Secondly, microgrid and cables are introduced in this chapter. The overall structure of the DC community microgrid is described. Modeling cable and deciding the parameters are described too. Both models in this thesis of microgrid and cable are presented.

3 The wavelet packet theory is introduced in the chapter. After introduction of classic Fourier transform, the wavelet and the traditional analysis using discrete wavelet are described. The advantage and usage of wavelet packet are presented.

4 The simulation and result analysis are shown in this chapter. Divided into two parts, the transient process and stable process are analyzed using traveling wave and impedance analysis respectively. Results, as some analysis are presented.

5 This chapter contains the conclusion and the future work, where the discussion of these method in the DC microgrid and the suggestions for implement in reality are obtained. There is some work that is valuable for the better location presented in the final.

Chapter 2 DC Microgrid and Cable

2.1 DC Microgrid

2.1.1 Microgrid Overall

This research is based on an existed DC microgrid plan [22]. As it mentioned in the first chapter, the system is built to help the transformation from a AC based community to a DC-enabled network. In that way, the DC microgrid in this concept cannot belong to a fully isolated running grid type. The structure be regarded as an upgrade of community grid while still connected to the AC utility grid. While introducing the DC source and DC loads, the traditional AC power source still are supplying the loads mainly under normal operation and AC loads still need the direct AC power feed instead of converter-inverter path.

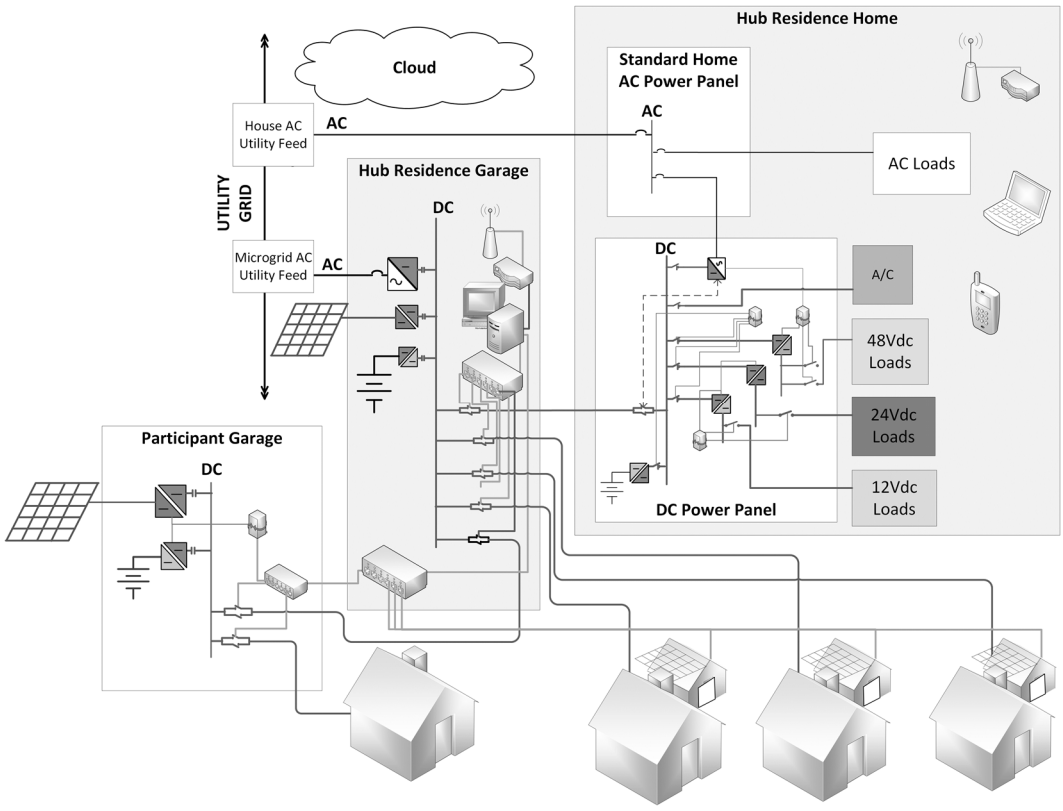

Figure 2-1 General Structure of DC Microgrid

Figure 2-1 shows the general structure of this DC microgrid. Three main district can be divided in this system as in grey background individually: Hub garage, participating garages, and hub houses. Every hub house has a corresponding garage in this case.

The hub garage part is the single part that attached with the AC utility grid in the system since the stable main power of DC microgrid can be feed by the AC power through the converter in normal operation. All the houses and participating garages are connected to the hub garage to have the AC-converted DC source. As a concentrated node, the hub also contains the renewable energy source such as PV panel, as well as energy storage device like batteries, where in figure it is drawn simply as a DC source. In the hub garage output terminal, there will be a panel which collects all the cable that link to all the participating garages like the center point of a star network. The participating garage is simplified version of hub garage where no connection to AC utility grid and

other participating garages exists. As notes in distributed renewable energy network, the PV panel and the batteries remains in the participating garage. All the garages are connected to the hub houses. There are AC and DC bus in the houses. AC bus feeds the AC load from AC utility grid and the DC bus. DC bus, with AC bus and batteries attached, feeds the DC loads through the necessary DC-DC converter if the level of voltage needs to be changed.

From the figure, we can still see the traditional AC power: the hub is directly connected to AC power utility grid; there are still AC loads that being feed from the AC power from both AC power panel and DC power panel through inverter. In the ideal running mode, a net-zero energy community can be achieved. The main energy is coming from the renewable distributed energy sources while the AC utility grid is a safe complimentary for the community and traditional source for certain AC equipment.

2.1.2 Simulation Approach and Implantation in Reality

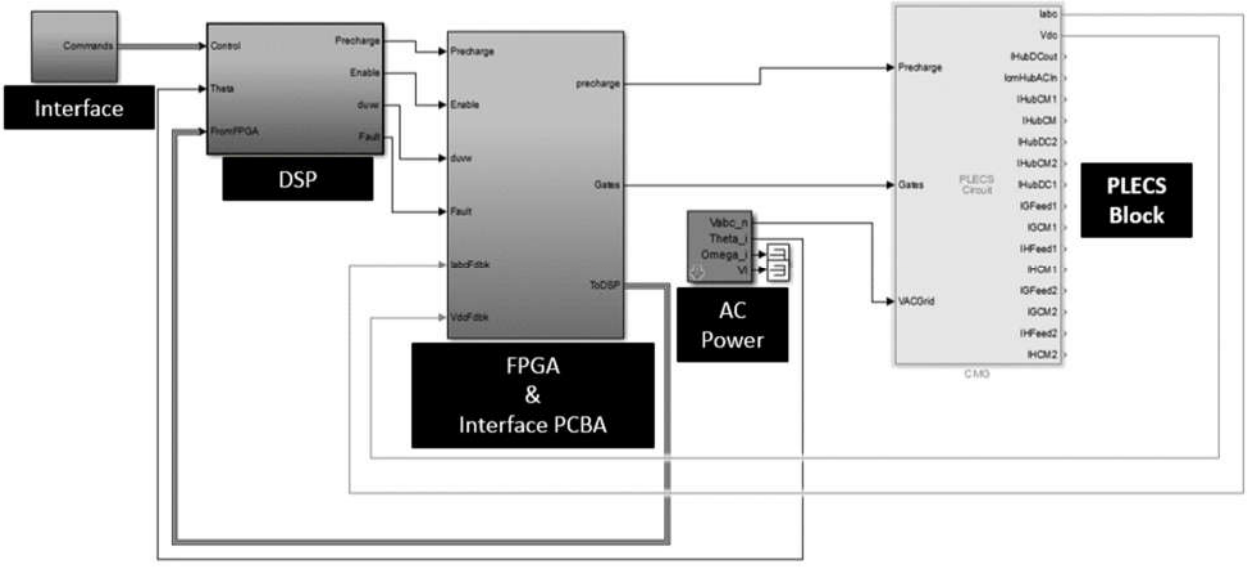

Figure 2-2 The Main Structure Shown in Simulink

The DC microgrid need a complicated but also easy-tweak simulation model to develop more researches. The Figure 2-2 is the simulation model that various control and situations can be simulated. The main frame is established in the Simulink as a visible simulation part in MATLAB, with main circuit set in a PLECS block. The system contains so many electronic devices (converters. Inverters, switches) that PLECS will be extremely suitable to implement. The PLECS also provide a seamless experience as intergraded part in the Simulink.

The interface simulates the various situation that the system may encounter and output the corresponding signal to the DSP block. DSP block contains a state machine, where the transformation of the system status can be decided by this part. The FPGA and interface PCBA is the block in charge of generating the control signals by feedbacks and commands. A careful and elaborate design is needed. The AC Power block simulates the AC utility grid with possible non-ideal options such as phase delay, unbalanced phase voltage and harmonic power components. The PLECS is connected in the end as equivalent DC microgrid.

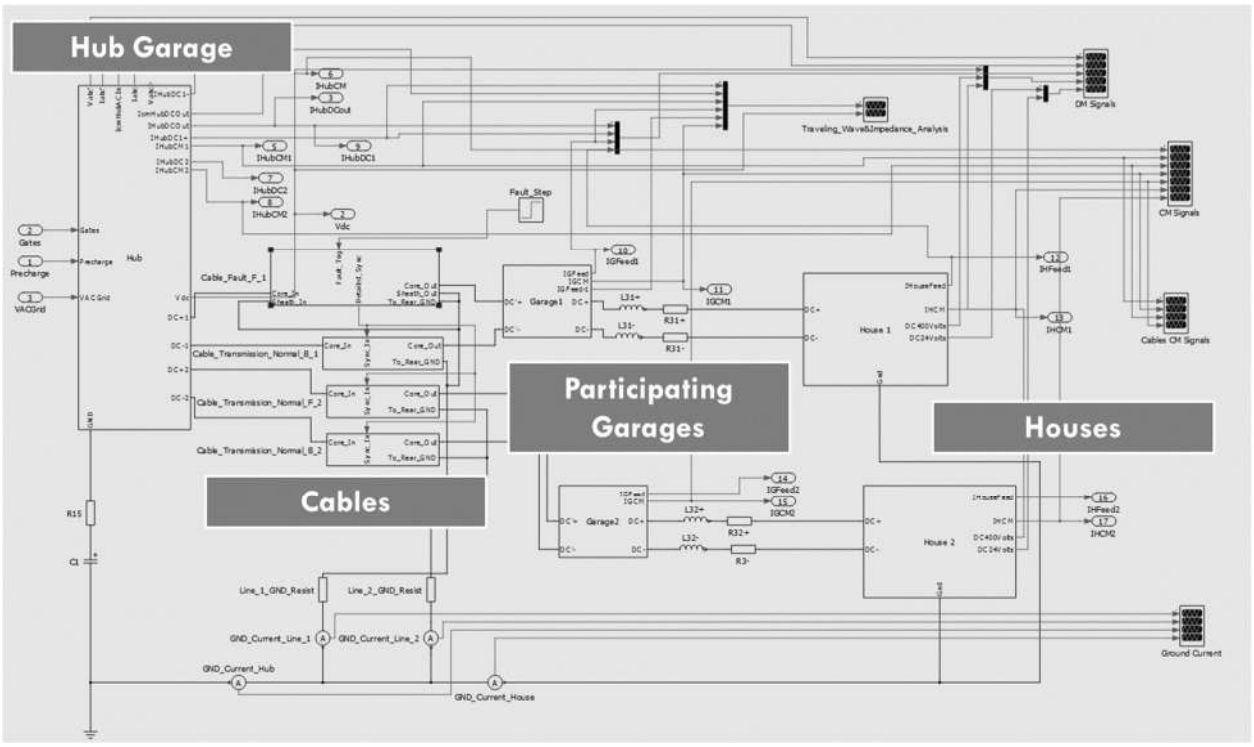

Figure 2-3 The Main Circuit in PLECS Block

The similar parts seen in the PLECS blocks in Figure 2-3 can be corresponded to Figure 2-1. The outside is connected to the hub garage and participating garages connect between the hub garage and houses. The user load is carrying by the houses. The main research part, in this article, exists between the hub and garages where cable blocks are built.

This microgrid system is planning to be implemented in rural area in Milwaukee. Milwaukee's Garden Homes community, which has several aged houses and its garages. The non-profit organizations will help rebuild these houses and garages to achieve the scheme of DC microgrid. With 230 volts AC and 380 volts DC inter-connected, these houses are expected to get effective and economic power grid with the same reliability requirement. This project will also have a positive impact on the education and societal aspects where people can see the advantages of DC microgrid in the real life.

2.2 Cables

Cables, usually buried cables, are considered as another common media for power transmission. Compared to transmission line, cables also contain several electrical conductors but usually are held together with an overall sheath. Cables can be installed as permanent wiring within buildings, buried in the ground, run overhead, or exposed. In this paper, the DC cables buried in the ground used for DC microgrid are analyzed.

Cables have a long history [23], started with the first power distribution system by Thomas Edison in 1880s, which is built with copper rods as core and wrapped in jute. Through hundreds of years, as the power transmission and distribution system fluently developed, the cables also had experienced several stages. Early cables are manufactured with core bare or cloth-covered with staples. Later, after 1880s, the knob-and-tube wiring standard were promoted where the cables are using asphalt-saturated cloth or rubber for insulation. In 1900s, the armored cables, which is famous by the brand "Bx", were introduced with flexible steel sheath and cloth-covered and rubber-insulated conductors with extra cost. In 1922, new cable type, which have the rubber-insulated wires but using jackets of woven cotton cloth and waxed paper filler was invented. The polyvinyl chloride-insulated (PVC-insulated) cable was introduced with the trademark "Romex" in 1950s. To reduce the cost, aluminum core was used as substitution of copper, which is proven not reliable later, started from 1960s. Modern three-wire thermoplastic-sheathed cable, like PVC-sheath covered type, have spread in the market for AC power transmission and distribution nowadays. As higher voltage cable need camp up with the development of high voltage (HV) applications, new materials have been applied to the cables, such as cross-linked polyethylene (XLPE). Not from the economy and performance side, but other factors push cables towards

upgrading too. The asbestos was popular in the cables but eliminated in the late 1970s due to the environment and health concerns.

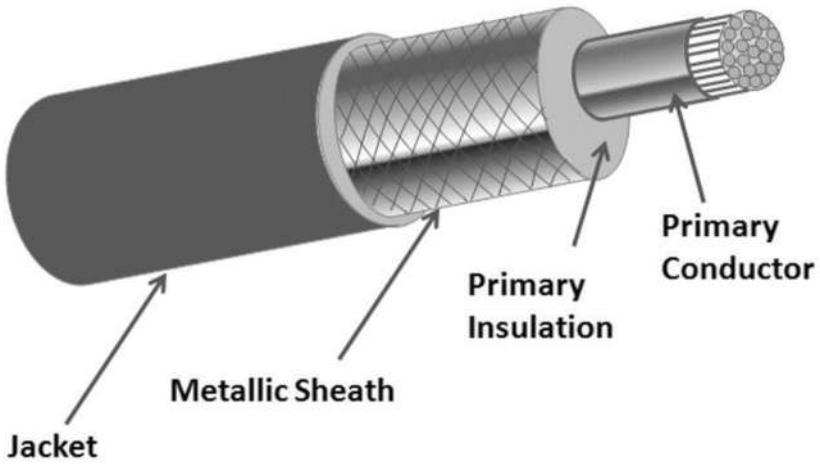

Figure 2-4 Structure of Cable

Most cables contain parts shown in Figure 2-4. The conductor carries the current delivering the energy. The insulation part, which may have more than one layer, protects the current from leaking electrically. The sheath, where can be metallic or non-metallic, help the cable maintain the shape and mechanical performance physically. The jacket covered as the outermost layer which helps to protect the wire from the external force and especially chemical deterioration in the first place. Higher voltage rating cables may have more complex structures than this. Some ultra-high voltage (UHV) cables contain semiconductor layers in order to prevent harmful electric discharges caused by the air-filled cavities.

Finally, IEC standard and other standards should be introduced. The IEC 60502 (Part 1) and IEC 60189 for the low voltage power cable (1kV – 30kV) and low-frequency cables and wires with PVC insulation and PVC sheath respectively can be used as reference. NEC (National Electrical Code) has some regulations too. But there is none such standard for DC especially for distribution wires in a low voltage level (e.g. below 1kV). For DC microgrid use, for safety reason, we can use the cable whose rating is degrading from a higher level of AC cable. The following part is the

introduction of cable parameters and the model that suit for methods applying in this paper during simulation.

2.2.1 Cable Selection

The main part of selecting the proper cable is based on where the cables are installed and how much the capacity it may carry as well as what type of current it will transport. As we are implementing cables in DC microgrid, where the cables are located underground and carries the direct current, the buried and DC cable can be selected in no doubt. Also, there is no issue about the parallel effect due to three phase power transmission which need transposition. For microgrid which is a complimentary term regarding to utility AC grid, the voltage should be much lower since no long-distance transmission is needed with current level being relative lower too. This means the capacity and the voltage-current rating for cable will be at bottom level compared to high voltage cables. The size, especially the sectional area, of the cable is small in result.

Power cables must have a service life of at least 15-20 years while carrying the expected load and overload current without overheating under worst ambient situations in a certain time. During its life time, cables also need to bear the mechanical stress as well as other interferences such as humility and radical impact.

Copper and aluminum are popular materials for core. But since people pursue more impact design in industries, copper becomes the main stream as it can carry 40% more current under the same sectional area. The sheath use aluminum in most situation as it is a balance of cost and performance. Three critical design criteria are involved: ampacity, sheath thickness and pulling tension when we select the cable specification.

There are several standards regarding the ampacity design of cables. IEC 60287 together with method of installation as documented in IEC 60364-5-52 can be used as reliable sources. The

ampacity is calculated based on the equilibrium temperature of the conductors when it can reach its maximum value like the NEC used in [24].

2.2.2 Cable Parameters

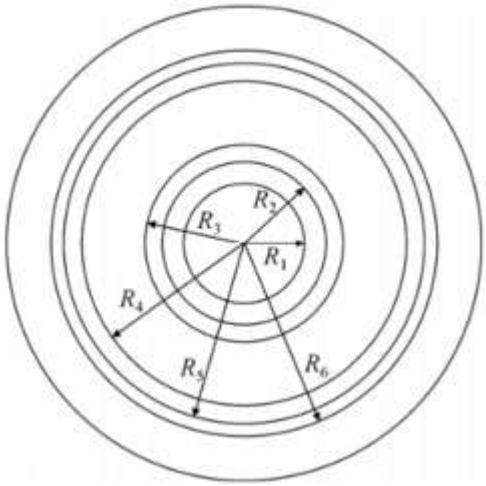

Figure 2-5 Vertical Profile of Single-core Power Cable

As shown in Figure 2-5, cables have multiple layers which have different functions. The two good conductor are core and sheath. Other parts have relatively extreme performance on insulation. Proper parameters are crucial to an effective analysis. Some basic parameter calculation is provided below where the key points that may influence can be seen.

a. Resistance

For power cables shown in Figure 2-5, the resistance per unit R_d under the temperature θ(℃) can be calculated by

$$R_D = \frac{\rho_{20}}{A}\big(1 + \alpha(\theta - 20)\big)k_1k_2 \qquad \text{Equation 2-1}$$

Where A is the sectional area, ρ_{20} is the electrical resistivity under the temperature 20℃, α is the temperature coefficient of conduct resistance, k_1 is the coefficient introduced from mechanical processing, and k_2 is tolerant factor.

For AC current, the cable core resistance will increase due to skin effect and proximity effect, so the corresponding coefficient should be applied like

$$R_A = R_D(1 + Y_S + Y_P) \quad \text{Equation 2-2}$$

Where Y_S is the skin effect coefficient and Y_P is the proximity effect coefficient.

For DC microgrid, the cable is designed to mainly carry the direct current instead of normal AC cables. But it should be noted that ripples in the steady operation and impulse in the transient process almost contribute to the AC part where the regarding resistance will change. In most situation these changes can be ignored because the absolute value of AC component in a relative long time takes the minor part.

The insulation resistance sometime is mentioned as below

$$Ri = \rho_v \frac{\delta}{S} \quad \text{Equation 2-3}$$

Where ρ_v is the coefficient of insulation resistance and δ, S is the thickness and electrode area individually. There is no further discussion about insulation resistance since in the following sections it is ignored in the simulation and analysis, because of its negligible affection.

When grounding fault or line short fault happened, the sheath and core are exposed to other conductor or earth in various situation, where some fault impedance, especially may be used to represent. This is discussed in later section.

b. Inductance

The inductance of cables is the ratio of the magnetic flux linkage of conductor and the current in the cable.

For pure DC current, after initial charging process, the inductance containing in the cable can be ignored. But the real situation is not that ideal, where the ripple from the converter and the variable load can lead to the non-dc component in the current. Also, the ground fault, which is main topic

of this article, will generate a transient situation that ambient frequency components will be included in the transient fault current, where the inductance of cables will be important factor to decide the values of the current in specific transient process. It is imperative to estimate the accurate inductance value to reach simulation result that comply with the real situation.

For normal cables, the induced voltage by magnetic field should be considered as the influence that induced voltage imposing to field can be ignored. It can be divided into two parts: the internal and external inductance, which corresponds to the internal flux and external ones individually. The external flux is coming from the other cable from the loop which usually carries the returning current.

For the internal part,

According to Ampere circuital theorem, we have

$$\oint_L H_i dl = I_i \qquad \text{Equation 2-4}$$

The perimeter is $2\pi X$, so

$$H_i 2\pi X = I_i \qquad \text{Equation 2-5}$$

And we can get

$$H_i = \frac{I_i}{2\pi X} = \frac{I}{2\pi X} \times \frac{X^2}{\left(\frac{D_e}{2}\right)^2} \qquad \text{Equation 2-6}$$

Where D_e is the diameter.

We know the energy of magnetic field for core conductor is expressed:

$$W = \int_0^D \frac{1}{2}\mu_0 H_i^2 \, dV = \int_0^D \frac{1}{2}\mu_0 H_i^2 \times 2\pi x dx \qquad \text{Equation 2-7}$$

As we know $W = \frac{1}{2} L_i I^2$ and we can put Equation 2-6 into Equation 2-7, then

$$L_i = \frac{\mu_0}{8\pi} = 0.5\times 10^{-7} \ H/m \qquad \text{Equation 2-8}$$

For the external part,

We can assume the current is concentrated around the central axis of the cable, so the magnetic field intensity of any position x where $x > Dc/2$ can be the superposition of two integration curve of magnetic flux.

$$H = H_A + H_B = \frac{I}{2\pi x} + \frac{I}{(2\pi(s-x)} \quad \text{Equation 2-9}$$

Where s is the distance from another cable central axis and I is the core current.

Then the magnetic flux can be calculated as

$$\phi = \int_s Bcos\beta ds = \int_{Dc/2}^{s} \frac{Dc}{2} \mu_0 H dx = \frac{\mu_0 I}{\pi} ln \frac{s - D_c/2}{D_c/2} \quad \text{Equation 2-10}$$

Normally the $D_c/2 \ll s$, so

$$\phi = \frac{\mu_0 I}{\pi} ln \frac{2s}{D_c} \quad \text{Equation 2-11}$$

So the external inductance will be

$$L_o = \frac{\phi}{2I} = \frac{\mu_0}{2\pi} \ln \frac{2s}{D_c} = (2 \ln \frac{2s}{D_c}) \times 10^{-7} \ H/m \quad \text{Equation 2-12}$$

The total inductance can be calculated as:

$$L = L_i + L_o \quad \text{Equation 2-13}$$

Unlike the AC power system implantation, for dc system, there is no need to use multi-core cables to carry the three-phase current in nearby conductor. The only possible source for external magnetic flux is coming from the loop cables carrying the returning current.

c. Capacitance

The cable itself can be seen as a cylinder capacitor. The conductor core and the metal sheath are the poles of a capacitor. The existence of capacitance can influence of the capacity and the length of the cable.

The capacitance calculation can be started with the electrical field. Ignoring the edge effect, using Gauss theorem, we have

$$\oint_S EdS = \frac{q}{\varepsilon_i} \quad \text{Equation 2-14}$$

So

$$E \times 2\pi x = \frac{q}{\varepsilon_i}$$

$$E = \frac{q}{2\pi x \varepsilon_i} \quad \text{Equation 2-15}$$

Where q is the electric charge that core contains, ε_i is the dielectric constant of the medium, E is the electric field density.

The voltage between this virtual capacitor can be calculated by

$$u = \int_l Edl = \int_{D_c/2}^{D_i/2} \frac{q}{2\pi x \varepsilon_i} = \frac{q}{2\pi\varepsilon_i} \ln \frac{D_i}{D_c} \quad \text{Equation 2-16}$$

Where D_i is the external diameter of insulation layer and D_c is the external diameter of conductor core. So the capacitance is

$$C = \frac{q}{u} = \frac{2\pi\varepsilon_i}{\ln\frac{D_i}{D_c}} = \frac{2\pi\varepsilon_0\varepsilon}{\ln\frac{D_i}{D_c}} \quad \text{Equation 2-17}$$

Where ε_0 is permittivity of vacuum ($\varepsilon_0 = 8.86 \times 10^{-12}\ F/m$) and the ε is the relative dielectric constant.

It can be simplified to

$$C = \frac{55.7\varepsilon}{G} \times 10^{-12} \quad \text{Equation 2-18}$$

Where G is the shape coefficient.

For multi-core cables, specific data sheet can be used to calculate the more accurate value of capacitance with certain coefficient multiplied. It will not be discussed here cause most DC cable used in microgrid is single core type.

2.2.3 Equivalent Circuit

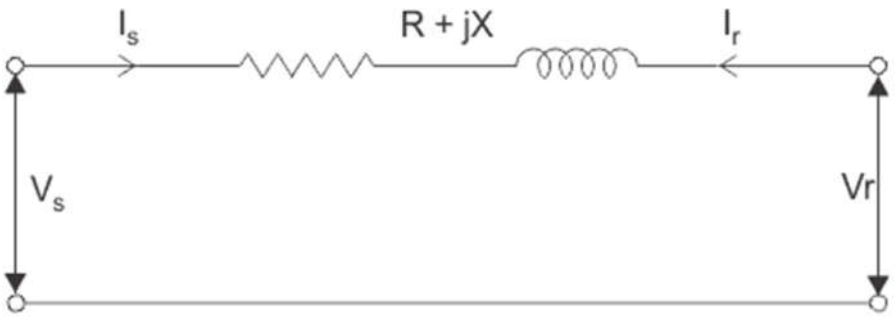

Figure 2-6 Simplified Model for Transmission Lines and Power Cables

Usually, we do not use very complex model for transmission lines and cables. The impedance and admittance per unit for them, especially the admittance towards the ground, are tiny. For most applications, these can be ignored. When the length is large enough, the impedance part, including the resistance and inductance, are considered to represent a line or cable model while the admittance part, including conductance and capacitance are still exempt. Figure 2-6 shows a simplified lumped (centralized) model of transmission lines or power cables which contains a resistor and an inductor. These two lumped components can represent most characteristics the cable may affect the system outside – the voltage drop, the loss and the non-liner process when alternating or unstable current flows through.

But when the parameters or characteristics inside the cable, transient situation like fault happened in cables, or the ground current that comes from the conductance of the cable becomes the target to be analyzed, it is necessary to introduce a more detailed model. There are various ways to model the cables more accurately, but T and π model, as well as distributed element model are reliable and widely used for detail simulations.

a. T Model and π Model

The idea for T or π model is to add the conductance into the model. This change gives the current, especially high frequency components new path to flow through. In most situations, the other side of conductance components are connected to real ground or chassis ground.

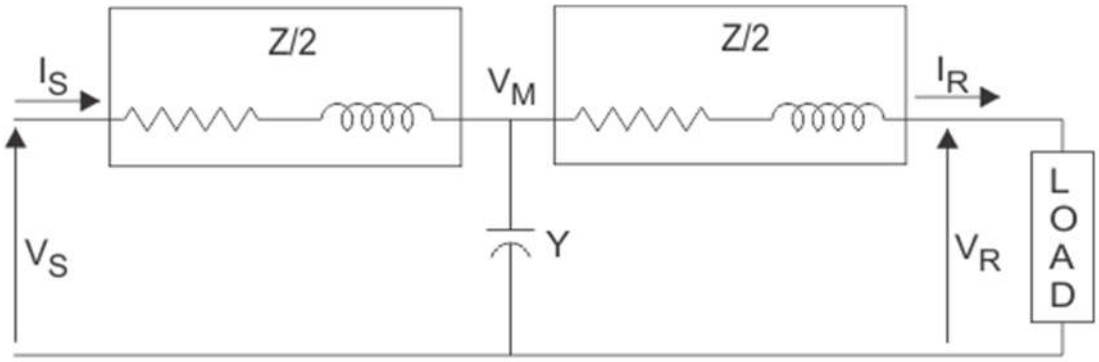

Figure 2-7 T Model for Transmission Lines and Power Cables

Figure 2-7 gives a typical T model for transmission lines and power cables. Notice in T model the whole shunt capacitance of line is assumed to be lumped at the middle of the line. The half of the line impedance is assumed at either side of the shunt capacitance. Due to such model, the capacitive charge current towards ground or neutral point is flowing the middle point of the cable.

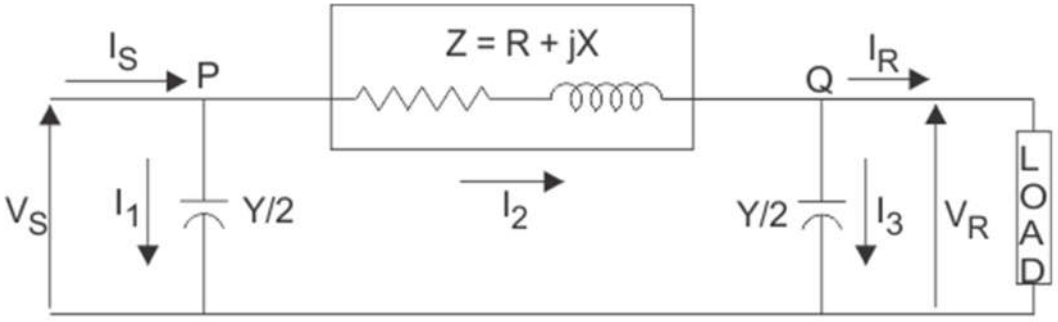

Figure 2-8 π(Pi) Model for Transmission Lines and Power Cables

More people nowadays use π(Pi) model which is shown in Figure 2-8 below. In π model, the shunt capacitance of each line towards ground or neutral point is divided into two equal parts. One part is lumped at the sending end while the other end is lumped at the receiving end. This model,

compared the T model, gives more information when the research focuses on the capacitance and the environment influence from the line. Note π model will give no effect at the sending end on the voltage drop but shows the charging current influence at the receiving end compared to T model.

Both T and π models are still considered as lumped parameter model though they do provide more detailed characteristics and can be used in several situations [25]. Before introducing the distributed parameters, a possible way to get an accurate model is to put these models in series. As we know later the distributed way can be seen as infinite π or T model in series, so more models you put in series to simulate a cable, more precise result is get, while you sacrifice for more time used to calculate. It depends on the balance of time and detail to make a smart choice. When you can afford the extreme time cost by high number of T/π sections, the distributed line model should be used instead.

b. Distributed Line Model

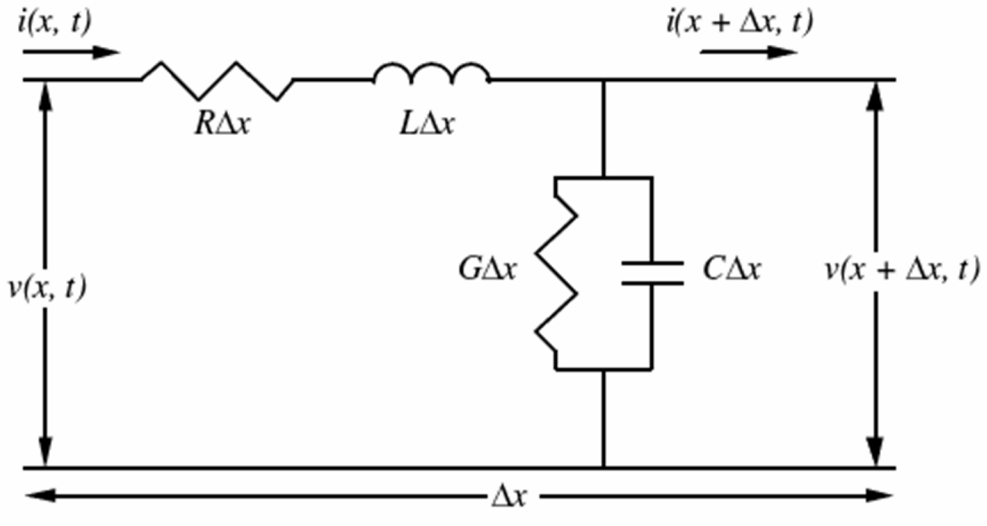

Figure 2-9 Distributed Element Model of Transmission Lines and Power Cables

Distributed element model is widely used in the Transmission Line Modeling Method (TLM) first but it applies for transmission lines as well as cables as it is shown in Figure 2-9. From the lumped model, it can be converted to the distributed element model if we assume there are infinite lumped components of T or π model. Ultimately, we can use the parameters per length element Δx to represent line. The resistance $R\Delta x$, the inductance $L\Delta x$, the conductance $G\Delta x$, and the capacitance $C\Delta x$ exist in every element per length. In the metric system we use ohms per meter (Ω/m), henries per meter (H/m), siemens per meter (S/m) and farads per meter (F/m). The good thing that distributed element model can provide is a way to connect the *E* and *H* field and the voltage-current in every point on the line. Some equations can be deduced from the model:

$$\frac{\partial v(x,t)}{\partial x} = -Ri(x,t) - L\frac{\partial i(x,t)}{\partial t} \qquad \text{Equation 2-19}$$

$$\frac{\partial i(x,t)}{\partial x} = -Gv(x,t) - C\frac{\partial v(x,t)}{\partial t} \qquad \text{Equation 2-20}$$

These differential parameters will be basis to develop the traveling wave theory.

2.2.4 Cable Model and Ground Fault in Cable Simulation

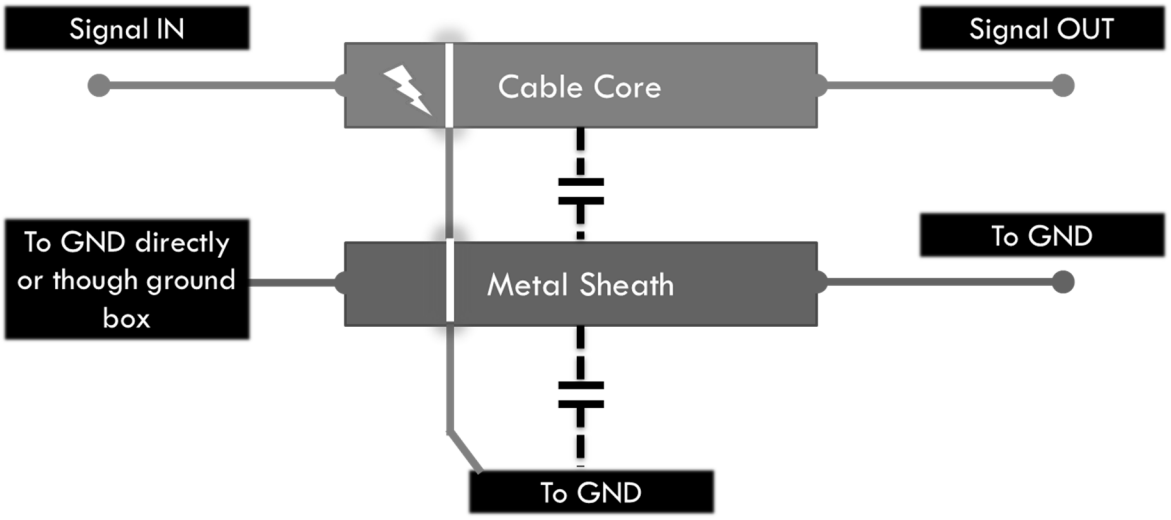

Figure 2-10 Cable Model Structure in General

As introduced in previous, if we ignore the influence of other insulation parts, the core and sheath are remaining two parts that need to be modeled. Five ports are in the model as shown in Figure 2-10, two for core, two for sheath and one for the common ground being set as the figure shows and distributed element models are applied in the core and sheath model. Instead of connecting ground by capacitor, when the ground happens, the core and sheath will be cut into two parts individually from the fault point and get short each other in same point.

The model achieved by PLECS can be seen below and switching of rough and detail model is introduced.

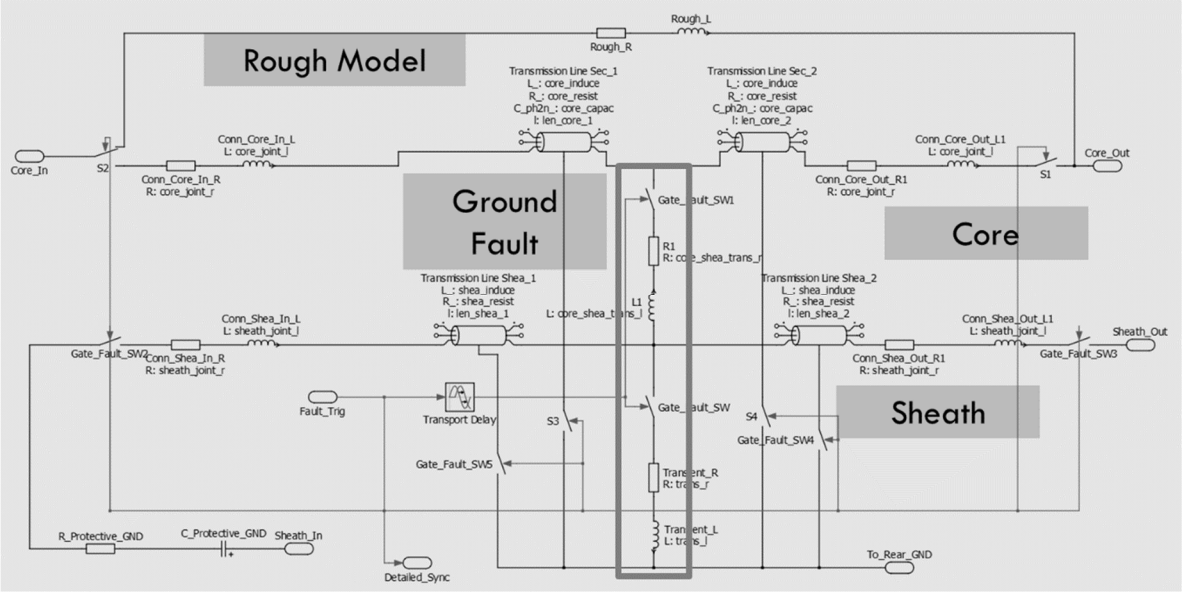

Figure 2-11 Ground Fault Simulated Cable Model

From the Figure 2-11, top part which is composed of a resistor and an inductor is the rough model. It is the same model that Figure 2-6 shows. In the start normal running procedure, it is unnecessary to put a complicated model into simulation as the computing capability is limited. This model will keep the system running normally and keep stable before a detail model switching in.

a. Detail Model

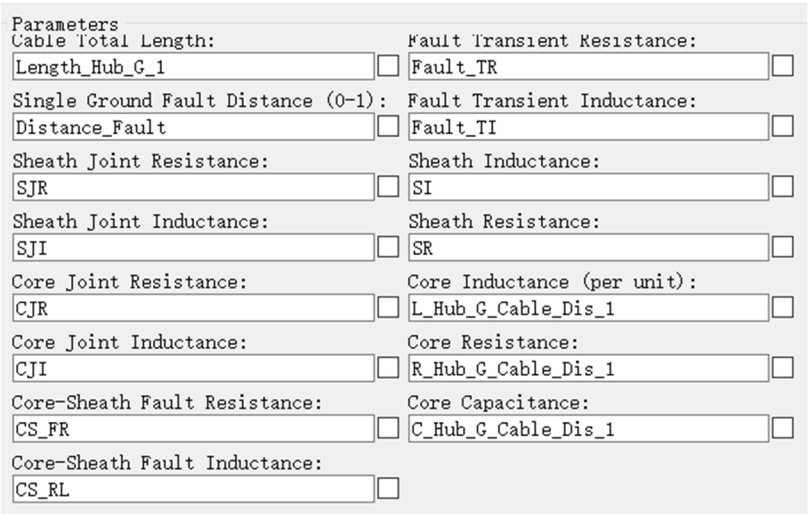

Figure 2-12 Parameters of Cable Model

The detail model is the rest part of Figure 2-11 except the ground fault box indicated in the middle. The core and sheath is using the similar model method by using the “transmission line” model in the PLECS libraries where it matches the model introduced in Figure 2-9. Joint resistance and inductance are considered in the input and output in both core and sheath. All parameters that can be set are shown in Figure 2.12, noted some or all parameters can be assigned to a certain variety that will be initialized in .m file when the simulation starts.

b. Ground Fault Simulation

The box in the middle consists the part of ground fault simulation. When the fault happens, switches turning on will create a new path for core and sheath current to flow through the ground. The transient impedance as well as the possible impedance between core and sheath in the fault point can be set as shown in Figure 2.12.

The switching signal is received by a step block where a delay transport is set to send the detail model switching model for certain seconds before the fault happens. The step block time and the detailed model delay time can be set in the PLECS block individually.

2.3 Signal Measurement in System

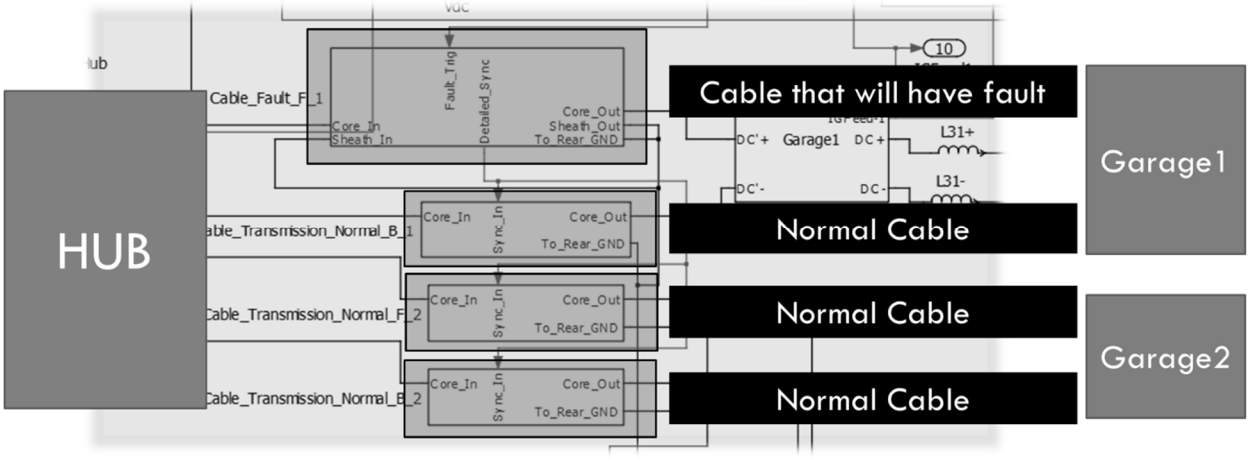

Figure 2-13 The Cable Models in the Microgrid PLECS Block

Figure 2-13 shows the connection of cables between the hub garage and the participating garage. Not putting the measurement in the cable model inside, measurements are putting outside in order to accord the real scenario in the hub and garage side. Measurement devices are considered ideal where no loss or interference exists. In most situation, there are two cables forming a loop connected between the hub garage and participating garage where input and output current flows separately. So the measurement of cables should always be deployed in pairs as the common mode (CM) or differential model (DM) measuring, and the signals of normal running cable will provide reference data at least.

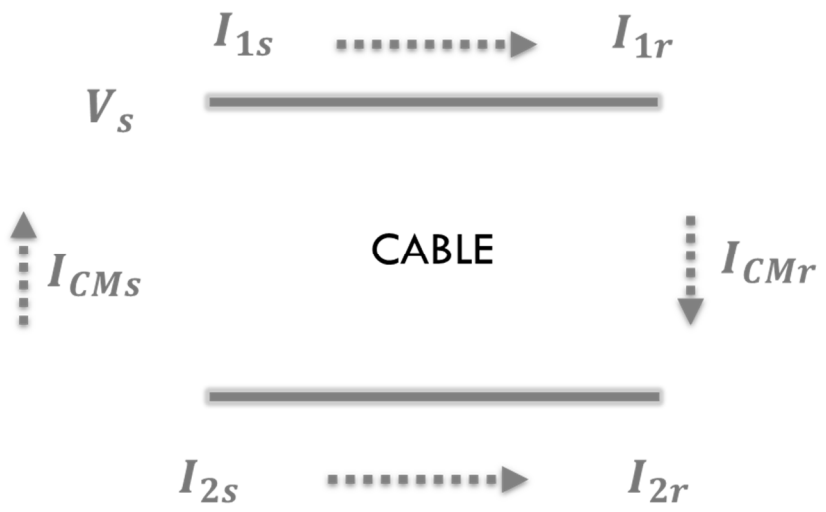

Figure 2-14 The Signals to be Measured around Cables

Table 2-1 The Signals that Measured in Microgrid System

Location	**Signals**
Hub	Sending End Current of Fault Cable
Hub	Sending End Current of Normal Cable(s)
Hub	Sending Point Common Mode Current
Hub	Sending End Voltage regarding to GND
Garage	Receiving End Current of Fault Cable
Garage	Receiving End Current of Normal Cable(s)
Garage	Receiving Point Common Mode Current

We are putting current and voltage sensors in these places as Figure 2-14 and Table 2-1 shows, noted that not all signals are using in the analysis because some of them are proven to be not helpful later. These sensors can not only provide information for the cable ground fault location, but also take even more responsibility in detecting the types of cables faults as well as the fault area in the whole system.

Chapter 3 Wavelet Packet

This chapter will introduce the time-frequency analysis methods. The Fourier transform is introduced first. Classical wavelet theory is described in detail. And the Wavelet Packet, as an improvement version of wavelet, is introduced last.

3.1 Time-Frequency Analysis and Wavelet Transform

3.1.1 Fourier Transform in Time-Frequency Analysis

In order to get better understanding about Wavelet transform, it is necessary to look into the history. The wavelet is developed through the process of researching and applying Fourier transform and seen as a milestone in 1980s.

As far as we know, Fourier analysis, including Fourier transformation and Fourier series, take a critical position in signal analyzing and processing. The reason that Fourier analysis has become an essential tool is it can redraw the characteristics in frequency domain from the time domain. The transformation between the time and frequency domain is convenient to achieve in theory and form, and the Fast Fourier Transform (FFT) makes its numerical implementation available in a satisfied speed [26].

Assume there is a time-domain signal $f(t)$ and its energy is limited, which can be describe as

$$f(t) \in L^2(R)$$

Where

$$L^2(R) = \left\{ f(t) \middle| \|f\|_0^2 = \int_R |f(t)|^2 dt < \infty,\ t \in R \right\} \qquad \text{Equation 3-1}$$

R is set of real numbers.

So, the Fourier and inverse Fourier transform can be applied as below

$$\begin{cases} \hat{f}(\omega) = \int_R f(t)e^{-i\omega t}\,dt, & \omega \in R \\ f(t) = \frac{1}{2\pi}\int_R \hat{f}(\omega)e^{i\omega t}d\omega, & t \in R \end{cases}$$ Equation 3-2

Noted that in Equation 3-2 the Fourier transform and its inverse version looks symmetrical in formula, then we can conclude it has some features like additivity and correlation. Especially, between these two equations there is one equation called Paseval:

$$\begin{cases} \int_R f(t)\overline{g(t)}dt = \frac{1}{2\pi}\int_R \hat{f}(\omega)\overline{\hat{g}(\omega)}d\omega \\ \|f\|_0^2 = \frac{1}{2\pi}\|\hat{f}\| \end{cases}$$ Equation 3-3

Combined Equation 3-1 and 3-2, it can be found that the Fourier transform and its inverse form is one-one corresponded, which means we can get the signal frequency characteristics $\hat{f}(\omega)$ from its time characteristics $f(t)$ easily, vice versa. The term Time-Frequency domain analysis is based on this property.

As for Fourier series, it could be the discrete form of Fourier transform. Any limited energy period signal in $[0,2\pi]$ can expand as Fourier series:

$$\begin{cases} f(t) = \sum_{n\in Z} C_n e^{int}, & Z\ is\ set\ of\ integers \\ C_n = \frac{1}{2\pi}\hat{f}(n) = \frac{1}{2\pi}\int_0^{2\pi} f(t)e^{-int}dt \end{cases}$$ Equation 3-4

Where $\{e^{int}\}_{n\in Z}$ is a set of orthogonal basis, and

$$\frac{1}{2\pi}\int_0^{2\pi}|f(t)|^2\ \ dt = \sum_{n=-\infty}^{\infty}|C_n|^2 < \infty$$ Equation 3-5

Fourier transform does can be used as a method for time-frequency analysis for signals, but it cannot localize any certain time-frequency part. In fact, if the goal is to fetch frequency information $\hat{f}(\omega)$ around a constant frequency ω, then all information from time domain $f(t)$ should be collected. But if part of frequency information is available, like certain band of frequency, the original information in time domain cannot be recovered. The signal changes in certain period can

affect all the characteristics in whole frequency domain, while signal changes in certain frequency bands can impact all characteristics in whole time domain.

We may focus its characteristics in local frequency scale for a local time domain based signal. For example, in power system fault signal analysis, we care about the transient time period that the fault current or voltage emerge and its corresponding frequency characteristics, trying to distinguish the fault type and the exact time. Common Fourier analysis cannot deal with issues like this, people require an innovative approach to analyze the short-time localization time-frequency information.

3.1.2 Classic Approach: Short Time Fourier Transform

Before the wavelet invented, a classic method to solve the problem is called Short Time Fourier Transform (STFT). It is defined as [27]:

$$f_{ab}(\omega) = \int_R f(t) g_a(t-b)^{i\omega t} dt \qquad \text{Equation 3-6}$$

Where $g_a(t-b)$ is called time windows function, which can limit the time domain signal into certain length period.

(6) is the equation to perform STFT for any signal which is already limited (multiply the $g_a(t-b)$). The function g_a has several choices, but it can be selected as Gauss function particularly, which is

$$g_a(t-b) = \frac{1}{2\sqrt{\pi a}} e^{-(t-b)^2/(4a)} \qquad \text{Equation 3-7}$$

Note that the Fourier transform of Gauss function is still itself, which means no matter in time or frequency domain, this function has the fast damping feature. This tells us Gauss can be used as a localization function in both domains, where people call it time-frequency window or double windows function.

From the window-featured STFT we can decompose the $\hat{f}(\omega)$, then get the local spectrum information, which is shown below:

$$\int_R f_{ab}(\omega)db = \hat{f}(\omega), \quad \omega \in R \qquad \text{Equation 3-8}$$

It should be noted that the STFT still has the same Paseval equation's feature, which proves this method can be implemented as a time-frequency transformation tools.

By identical deformation, we can get two important parameters for the windows in time and frequency domain: the center of window and the radius of window, which is shown below:

$$\begin{cases} t^*(g_a(0-b)) = b \\ \Delta\big(g_a(t-b)\big) = a \end{cases} \qquad \text{Equation 3-9}$$

$$\begin{cases} t^*(g_{1/(4a)}(0-\omega)) = \omega \\ \Delta\left(g_{1/(4a)}(\eta-\omega)\right) = \frac{1}{2\sqrt{a}} \end{cases} \qquad \text{Equation 3-10}$$

The Equation 3-9 and Equation 3-10 tell us the local information of $f(t)$ in time domain window $\left[b-\sqrt{a}, b+\sqrt{a}\right]$, can be observed in the window $\left[\omega-\frac{1}{2\sqrt{a}}, \omega+\frac{1}{2\sqrt{a}}\right]$ of $\hat{f}(\eta)$ in frequency domain. So, the square time-frequency window below

$$\left[b-\sqrt{a}, b+\sqrt{a}\right]\times\left[\omega-\frac{1}{2\sqrt{a}}, \omega+\frac{1}{2\sqrt{a}}\right] \qquad \text{Equation 3-11}$$

shows the scale of the processed signal in localization time-frequency domain, which depicts in Figure 3-1.

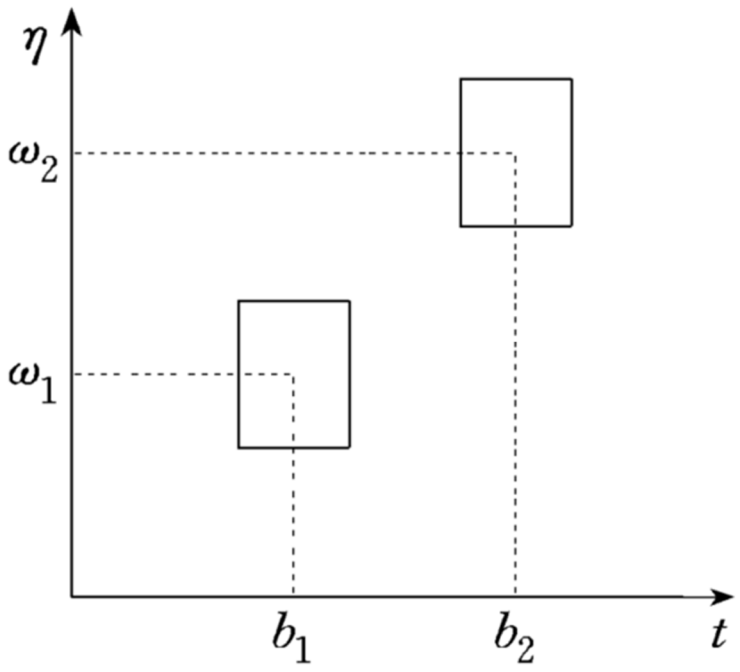

Figure 3-1 The Time-frequency Windows of the STFT

As an improved method, STFT satisfy some requirement for the users that need localization data in time-frequency domain. But it should be noticed that by the same parameters and function selected, the STFT will maintain unchanged windows, where the width values of time and frequency windows are constants. This disadvantage limits the STFT for precise analysis application. If we want to analyze information in high frequency band in certain period time, the narrower time-domain window and wider frequency-domain window should be selected; otherwise if the low frequency band contains the information you are interested in, wider time-domain window and narrower frequency-domain should be picked. STFT cannot meet some actual applications that need an adaptive and adjustable time-frequency window.

3.1.3 Wavelet and Adjustable Time-Frequency Window

To improve the performance of STFT, we hope a new transform method will not only have similar feature compared to Fourier and inverse Fourier transform, and the feature where can process information in time-frequency windows, but also can adjust the width of the windows. For this novel integral function performing transformation, we call it the Wavelet function [28].

Define a function $\Psi_{ab}(t) \in L^2(R)$, and this function may look like this:

$$\Psi_{ab}(t) = |a|^{-\frac{1}{2}}\psi\left(\frac{t-b}{a}\right) \quad \text{Equation 3-12}$$

And it must satisfy the admissibility condition:

$$C_\psi = \int_R \frac{|\hat{\psi}(\omega)|^2}{|\omega|} d\omega < \infty \quad \text{Equation 3-13}$$

We call $\Psi_{ab}(t)$ an admissibility wavelet, or basic wavelet. Then we define the wavelet transform below from the book [29]:

$$W_\psi f(a,b) = |\omega|^{-\frac{1}{2}} \int_R f(t)\,\overline{\psi\left(\frac{t-b}{a}\right)}\,dt \quad \text{Equation 3-14}$$

$$a, b \in R, \quad a \neq 0$$

Obviously, from its equation we can see the scaling and translation features, which will limit the time and frequency of signals the condition Equation 3-13 guarantee the wavelet function $\Psi_{ab}(t)$ and its frequency form $\widehat{\Psi}_{ab}(\omega)$ have the fast damping feature, where $\Psi_{ab}(t)$ and $\widehat{\Psi}_{ab}(\omega)$ can be used as time window and frequency window separately. Additionally, $\Psi_{ab}(t)$ is oscillatory and appears similar to some damping wave function, that is why it is called wavelet.

The wavelet defined by Equation 3-15 and 3-16 have similar features that Fourier transform has:

$$f(t) = \frac{1}{C_\psi}\int_R \int_R \left(W_\psi f\right)(a,b)\psi_{ab}(t)\frac{1}{a^2}dadb \quad \text{Equation 3-15}$$

$$\frac{1}{C_\psi}\int_R \int_R \left(W_\psi f\right)(a,b)\overline{\left(W_\psi g\right)(a,b)}\frac{1}{a^2}dadb = \int_R f(t)\overline{g(t)}dt \quad \text{Equation 3-16}$$

Once $\Psi_{ab}(t)$ is used as time window function, we can calculate the radius and the center point as below:

$$t^*\left(\psi_{ab}(t)\right) = at^*_{psi} + b \quad \text{Equation 3-17}$$

$$\Delta\left(\psi_{ab}(t)\right) = a\Delta_{\psi} \quad \text{Equation 3-18}$$

And for $\widehat{\Psi}_{ab}(\omega)$ as frequency window function, we can derive the radius and center point too:

$$\omega^*\left(\widehat{\Psi}_{ab}(\omega)\right) = \frac{1}{a}\omega^*_{psi} \quad \text{Equation 3-19}$$

$$\Delta\left(\widehat{\Psi}_{ab}(\omega)\right) = \frac{1}{a}\Delta_{\psi} \quad \text{Equation 3-20}$$

So we can list the rectangle time-frequency window below:

$$\left[\mathrm{b} + \mathrm{a}at^*_{psi} - a\Delta_{\psi}, \mathrm{b} + \mathrm{a}at^*_{psi} - a\Delta_{\psi}\right]\times[\frac{1}{a}\omega^*_{psi}\text{-}\frac{1}{a}\Delta_{\psi}, \frac{1}{a}\omega^*_{psi} + \frac{1}{a}\Delta_{\psi}]$$

Equation 3-21

This time-frequency window has its importance by showing us the feature it can adjust automatically. When processing high frequency bands, where a is relatively small, the window will become narrow; for low frequency bands, where a is relatively large, the window will become wide. This feature shown in Figure 3-2 highlights the use of wavelet when dealing with the sudden change signals.

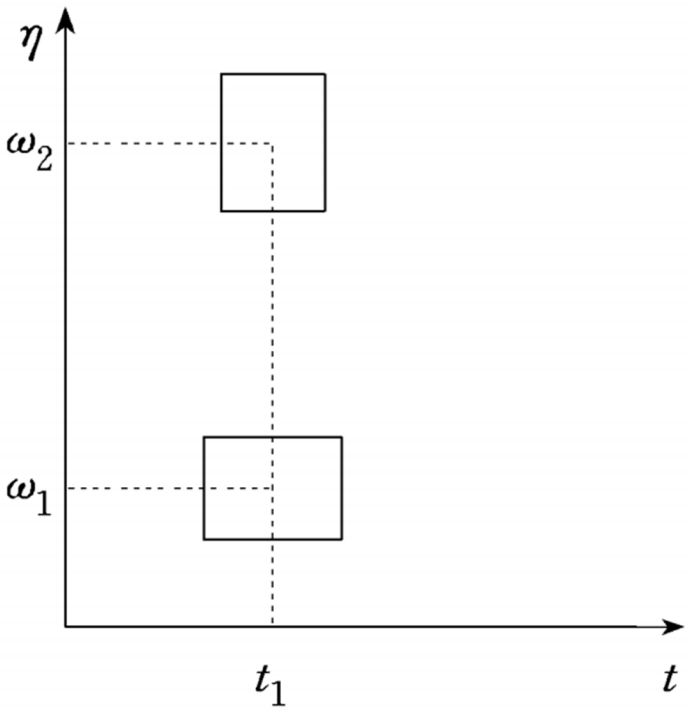

Figure 3-2 The Time-frequency Windows of the Wavelet

The a and b, as the parameters of wavelet transform, can be specialized in certain format to achieve designated goals. Also, the function of wavelet function is not exclusive, various wavelet function can be useful for different cases. That is why there are so many wavelet transform types. When we have a well-defined wavelet function ψ_{ab}, we can use wavelet transform to overcome the deficiency of classic Fourier transform family methods but keep their advantages. The core of wavelet is its adjustability, and with multiple advanced algorithm, wavelet analysis has taken crucial position into more science fields.

3.2 Applying the Wavelet Transform

3.2.1 Types of Wavelet Transform

We can directly use the wavelet transform formula shown in last section, but in reality it may be hard for cases under certain condition. Some wavelet methods have been developed to accord the signal input, calculating limitation, as well as application goals.

In general, there are following types of wavelet transform below in industry: Continuous Wavelet Transform (CWT), Discrete Wavelet Transform (DWT), Dyadic Wavelet Transform, and Stationary Wavelet Transform (SWT).

a. Continuous Wavelet Transform (CWT)

By using the basic formula that is shown in Section 1 of this chapter, the signal can be transformed into frequency-domain with time window embedded. Rewrite the formula below:

$$\Psi_{ab}(t) = |a|^{-\frac{1}{2}}\psi\left(\frac{t-b}{a}\right) \qquad \text{Equation 3-12}$$

In this formula, we call a as the scale parameter, and b as translation parameter. The scale parameter is closely related to the frequency, and the translation is related to the time.

b. Discrete Wavelet Transform

We cannot exactly perform Continuous Fourier Transform (CFT), due to impossibility to process a "real" continuous data steam in a digital processing based computer. Discrete Fourier Transform had been created for convenient application based on computer equipment. For the same reason, the discrete wavelet transform is developed.

Using the same formula as CWT, the only difference for DWT is that it adds the limitation to the parameter a and b. It needs the both parameters being discrete, which will lead to the all discrete

time and frequency windows in the transform. It should be noted that the time t is not been discrete, which is totally different to DFT.

The a and b should be set as certain values. Practically, for the scale parameter a, we make it discrete into power series like $a = {a_0}^m$. But for b we make it unique discrete. Noted that for different frequency dimension, the interval for every time point is changed.

c. Dyadic Wavelet Transform

As mentioned below, for Discrete wavelet transform, both parameters a and b are set to be discrete. So, what if we just make one of parameters be discrete and keep the other one continuous? We call this transform the dyadic wavelet transform. We make scale parameter a discrete in power series, which means ${a_0}^m$ (for special we even can select $a_0 = 2$). In general, the dyadic wavelet transform falls in between of CWT and DWT: it is especially discrete for one parameter compared to CWT, and its discrete method for one parameter is not arbitrary and the other parameter stays continuous compared to DWT.

d. Stationary Wavelet Transform (SWT)

It is known by people who use DWT, that DWT will lose its translation-invariant due to the downsampling process during the transform. In order to get translation invariant, stationary wavelet transform(SWT) is introduced. The difference of SWT and DWT is, instead of downsampling, the internal high and low frequency filter will proceed upsampling to get redundant data. This method will make the computation heavier but just need to tweak the original DWT algorithm.

SWT is extensively used in signal denoising application as well as signal regeneration. And there are other similar methods, which is variant version that substitute the downsampling procedure in

DWT. Some important methods include Maximal Overlap Discrete Wavelet Transform (MODWT), Undecimated Wavelet Transform(UWT) and so on.

3.2.2 Selection of Mother Wavelet

As mentioned in previous text, different from the Fourier transform, the wavelet transform need a wavelet function, as it is called mother wavelet, which is not exclusive. With the continuously development of wavelet research, various mother wavelet emerged. Which wavelet basis is suitable becomes a crucial question. In this section, some characteristics of mother wavelet are presented with certain common ones introduced.

There are several distinguishing characteristics that will help us decide which mother wavelet should be selected as the basis for wavelet transform.

a. Support length

The support length is defined that the length needed for wavelet function $\psi(t)$ or $\psi(\omega)$ converging to zero from a limited value when the time or frequency tends to be infinite. The longer support length, the more time it will take for calculation with higher amplitude of wavelet coefficients. Normally, the support length between 5-9 is applied for most applications. Inappropriate long support length will lead to boundary issues and short support length will result in bad concentration of signal.

A term intense support may be used to represent that the mother wavelet stay its value zero except an extreme tiny area around 0 for x.

b. Symmetry

Symmetry means the mother wavelet will have a liner phase characteristic, which will be an advantage in image processing and other applications to prevent the distortion.

c. Vanishing Moments

In practical, we do not only require the mother wavelet have admissibility condition (Equation 3-13) but also restrict its vanishing moments. With higher value of vanishing moments, there will be less non-zero wavelet coefficients, which will benefit in compression and denoising. But the better vanishing moments condition often comes with a longer support length, which make us must compromise in some degree.

The vanishing moments is defined as if the statement below exists,

$$\int t^p \psi(t) dt = 0 \qquad \text{Equation 3-22}$$

Where $\psi(t)$ is mother wavelet and $0 \leq p < N$. Then we call this basic wavelet function N_{th} order mother wavelet. It also means that there are high order zeros in frequency domain.

d. Regularity

When the wavelet coefficients being quantified or rounding off, to avoid massive change from its appearance human observing, it is necessary to enhance the smoothness or continuous differentiability. The mother wavelet which has better regularity, the result that being transformed will have a better look on transition.

As the regularity gets better, the support length will be extended which will result in longer calculation time. And there is relation between vanishing moments and regularity too, where the vanishing moments grows as regularity being improved for most important mother wavelet. In general, this typically shows that it is a comprehensive decision to get the suitable parameters for each case.

e. Similarity

It will get better compressing and denoising performance as well as other advantages when the mother wavelet is similar to the input signal.

Some useful basic wavelets are introduced below.

a. Haar

Haar is the first used wavelet which have the characteristics of compact supported and orthogonal. The equation of Haar wavelet is simplest. The definition is

$$\psi(t)\begin{cases}1, & 0 \le t < 0.5\\ -1, & 0.5 \le t < 1\\ 0\ , & otherwise\end{cases} \qquad \text{Equation 3-23}$$

It should be noticed that it is not continuous in the time domain, so its performance is fair. But it has its own advantages: simple calculation, orthogonality and others.

b. Daubechies (dbN)

Daubechies is created by the famous scientist Inrid Daubechies, abbreviated as dbN, where N stands for the order. dbN wavelet have a support length of *2N-1*. dbN do not have a certain equation (except N=1), but the function $|h^2|$ is known, which is

$$|m_0(\omega)|^2 = (\cos^2\frac{\omega}{2})\sum_{k=0}^{N-1} C_k^{N-1+k}(\sin^2\frac{\omega}{2})^k \qquad \text{Equation 3-24}$$

It should be noted that db1 is the Haar wavelet. For dbN wavelet, some characteristics show its performance in application. It is limited supported in time domain, and has Nth order zeros when $\omega = 0$. Also itself and its integer shift are orthogonal, as $\int \psi(t)\psi(t-k)dt = \delta$. More, the wavelet can be obtained by transform from scaling function $\phi(t)$, which is low pass and has support range from 0 to *2N-1*.

c. Meyer

Meyer wavelet is defined in frequency domain for itself as well as its scaling function.

$$\begin{cases} \frac{1}{\sqrt{2\pi}}\sin\left(\frac{\pi}{2}v\left(\frac{3|\omega|}{2\pi}-1\right)\right)e^{j\omega/2}, & \frac{2\pi}{3}<|\omega|<\frac{4\pi}{3} \\ \frac{1}{\sqrt{2\pi}}\cos\left(\frac{\pi}{2}v\left(\frac{3|\omega|}{2\pi}-1\right)\right)e^{j\omega/2}, & \frac{4\pi}{3}<|\omega|<\frac{8\pi}{3} \\ 0, & otherwise \end{cases}$$ Equation 3-25

Where $v(a)$ is an auxiliary function.

It should be noted that Meyer wavelet is not compact supported but it did have a high convergence speed. In time domain, we have

$$|\psi(\omega)| \le a^4(35-84a+70a^2-20a^2) \ , a \in [0,1]$$ Equation 3-26

So the function can be differentiated everywhere.

3.2.3 Orthogonal Wavelet Transform and Mallat Algorithm

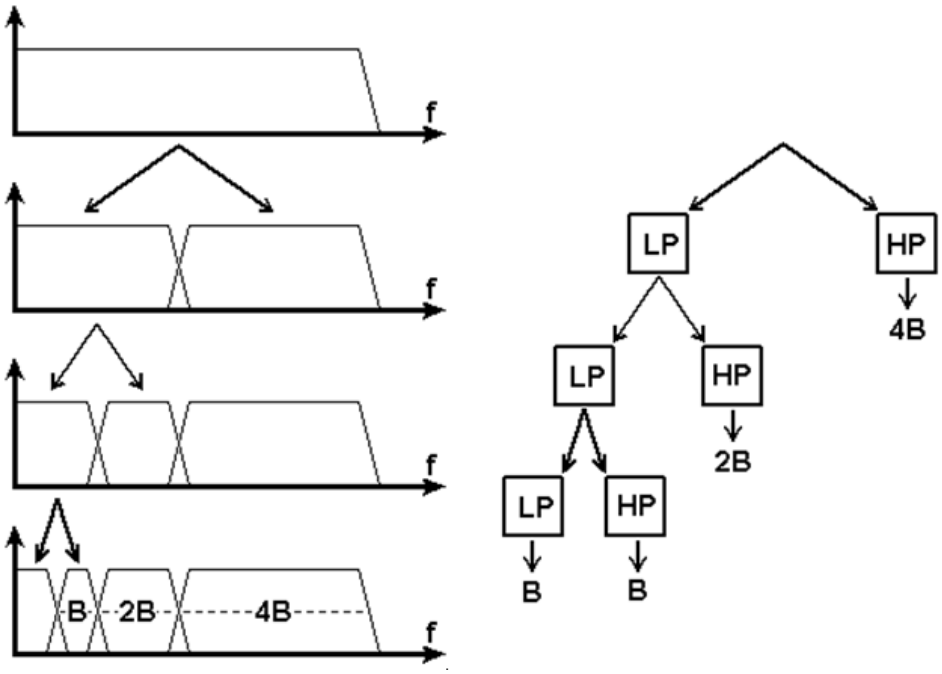

Figure 3-3 Frequency Bands Separation and multi-resolution analysis (MRA)

In practical application, due to the limitation that computer will use digital sampled data in the calculation, it should be focused on how to use the wavelet tools to analyze a discrete series data, which is similar to discrete Fourier transform. One feature that we need is Multi-Resolution

Analysis (MRA) shown in Figure 3-3, which a practical method to decompose the discrete series data should be introduced below.

At first, orthogonal wavelet transform should be introduced. When non-orthogonal basic wavelet is selected, the information after transformation is redundant. Mallat introduced a famous signal decomposition algorithm which is named by himself based on orthogonal mother wavelet.

Normally the wavelet transformation of discrete series we called is based on the Mallat algorithm. It should be noted that the Mallat algorithm is also applicable for continuous signals.

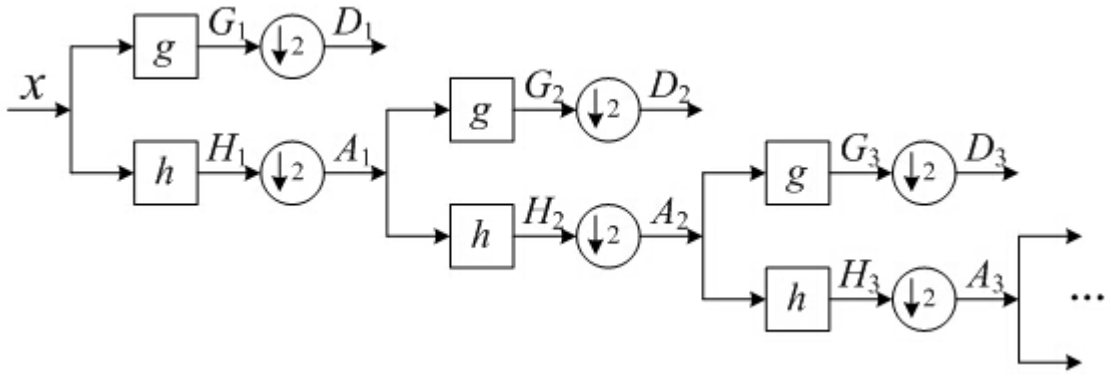

Figure 3-4 Mallat Algorithm Flow Chart

From Figure 3-4 we can explain the procedure of proceeding a wavelet decomposition using Mallat algorithm. The original wavelet coefficients data x is decomposed by layers, which accords to the term of scale. The relationship of high-frequency coefficients D_1 (D stands for Detail) of first layer and the x is that x is been through a high frequency filter g and a downsampling procedure then D_1 is generated, while the low-frequency coefficients A_1 (A stands for Approximate) generated through a low frequency filter h and a downsampling procedure of x. Then A_1 is being under second-layer decomposition (if more than two-layer decomposition requested) through the same method into high frequency coefficients D_2 and a low frequency coefficients A_2 while D_1 remains unmodified. Because downsampling is implemented every step, the filtering band is halved though the parameters of filter g and h do not change. When the requested decomposition

layer is finished, we can reconstruct the discrete signal using these decomposed coefficients which contains information from different frequency bands by orthogonal basic wavelet.

3.3 Wavelet Packet Decomposition (WPD)

One advantage of using wavelet transform is getting an adjustable tool which can get information from different frequency bands in frequency domain. But from Mallet algorithm we may found the only lower frequency band is continued to next decomposition with higher band stays original, which can be found in Figure 3.3. The result is, when decomposition is finished, all the bands have different length (except the last two) and the length increase as the frequency becomes higher. As after normal discrete wavelet transform, there will be relatively lower resolution in high frequency bands.

It is pointed it may be more appropriate to decompose both coefficients instead of only the lower frequency coefficients. Therefore, for certain signals, there is possibility that more valuable information exists in high frequency bands. People try to find an optimal method to decompose the low and high frequency coefficients in the same time based on designed criteria and this method is named Wavelet Packet Decomposition(WPD) [30].

Wavelet packets is also called Optimal Subband Tree Structuring (SB-TS). Simply to describe, the WPD will let the signal pass more filters than the discrete wavelet transform. The WPD will decompose the signal under arbitrary time-frequency resolution into different frequency bands and project time components of signal into orthogonal wavelet space which represent different frequency bands accordingly.

Define u_t function which satisfies

$$\begin{cases} u_{2n}(t) = \sqrt{2}\sum_{k\in Z} h(k)u_n(2t-k) \\ u_{2n+1}(t) = \sqrt{2}\sum_{k\in Z} g(k)u_n(2t-k) \end{cases} \quad \text{Equation 3-27}$$

Where $g(k) = (-1)^k h(1-k)$

The new series created from (3.xx) is called orthogonal wavelet packet determined by

$u_0(t) = \phi(t)$.

Then signal wavelet packet will be

$$g_j^n(t) = \sum_l d_l^{j,n} u_n(2^j t - 1) \quad \text{Equation 3-28}$$

Where $d_l^{j,n}$ is the coefficients from decomposition.

And the decomposition algorithm will be

$$\begin{cases} d_l^{i,2n} = \sum_k a_{k-2l} d_k^{j+1,n} \\ d_l^{i,2n+1} = \sum_k b_{k-2l} d_k^{j+1,n} \end{cases} \quad \text{Equation 3-29}$$

And the wavelet packet reconstruction algorithm will be

$$d_l^{j+1,n} = \sum_k (h_{l-2k} d_l^{j,2n} + g_{l-2k} d_l^{j,2n+1}) \quad \text{Equation 3-30}$$

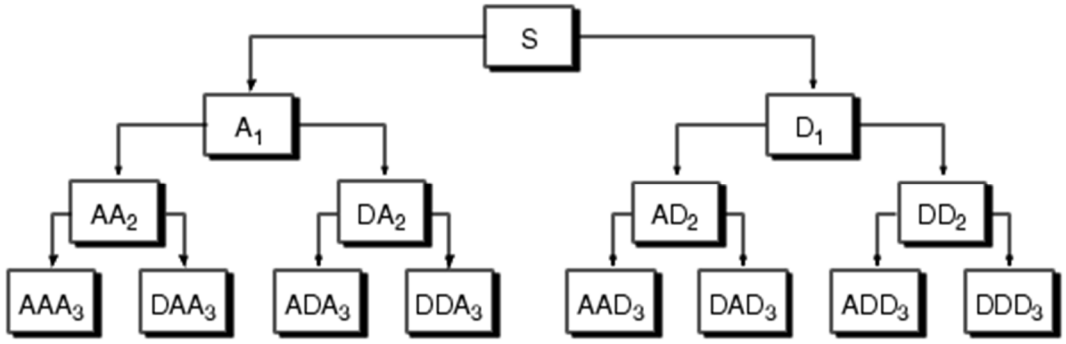

Figure 3-5 Frequency Bands Using Wavelet Packet

In general, using the wavelet packet, the signal will be synchronously decomposed like a tree, which is shown in Figure 3-5.

It should be noted that during the composition in high frequency band, the alias will happen. The reason is because the downsampling let the sample frequency gradually smaller, and then the sample frequency arrives certain value according to Nyquist theorem will lead to the alias phenomenon. This can be fixed by frequency shift operation.

Chapter 4 Simulation Result and Analysis

This chapter presents the result of simulation of two methods to locate the fault. The wavelet packet is applied on both methods.

4.1 System Overview

Based on the DC microgrid described in Chapter 2, which already existed in Milwaukee area and its future development, we can assume the proper cable specification as well as its parameters which will be used in simulations.

From the system power prediction table from the reference paper [22], we can calculate the assumed peak power needed (considering the DC voltage rating from the Hub is 400 Volts) for a house is

$$I_{peak} \cong 60A$$

$$P_{peak} \cong 400 * 60 = 24kW$$

From the electrical standards and the community construction handbook, also considering the safety factor, the 16mm^2 sectional area (AWG 5) copper conduct with aluminum sheath cable, which can carry more than 100 amps, is selected. The sheath thickness is assumed to be 0.5mm as recommended in IEC 60502.

In this paper, cables connected between the hub garage and the participating garage are using the same parameters while assigned to different length. The data is set regarding the real situation and simplified. Other cables in the system are not using the detailed model since the length of them are relatively short (smaller than 50m). The fault cable detection is not considered in this paper as there are other researches using wavelet method to distinguish which cables are in fault status.

Table 4-1 Cable and System Parameter

Parameter $(t = 20℃)$		**Value**
Cable Core	**Resistance**	$1.15\times10^{-3}\ \Omega/m$
	Inductance	$3.3\times10^{-7}\ H/m$
	Capacitance	$1.35\times10^{-9}\ F/m$
Cable Sheath	**Resistance**	$3.12\times10^{-2}\ \Omega/m$
	Inductance	$3.7\times10^{-5}\ H/m$
	Capacitance*	$1\times10^{-10}\ F/m$
Simulation Model	Distributed Element Model in PLECS Library	
Length of Fault Cable	$411\ m$	
Length of Normal Cable	$358\ m$	
House Load	$0.154\ \Omega\ /\ 0.105\ \Omega$ (House 1 / House 2)	
Converter Switching Frequency	$15000\ Hz$	
DC Feed Voltage	$380\ V$	
Detailed Model Switching In	$0.9\ s$	
Fault Happen Time	$1.0\ s$	

*The value of capacitance of sheath is set to complete the model, where the capacitance influence is ignored.

The Table 4-1 present parameters of the cable that need to be fault located we used in the model. This data is extracted from a user manual of cables. This table also provides some parameters of the DC community microgrid system. There are two participating houses along with garages in the model, which are using different parameters to avoid result due to balance situation.

Two analysis for transient and stable process analysis are shown in next two sections. Both two approaches use wavelet as the important signal processing method.

4.2 Transient Analysis Using Traveling Wave

4.2.1 Simulation Result and Effect of Traveling Wave

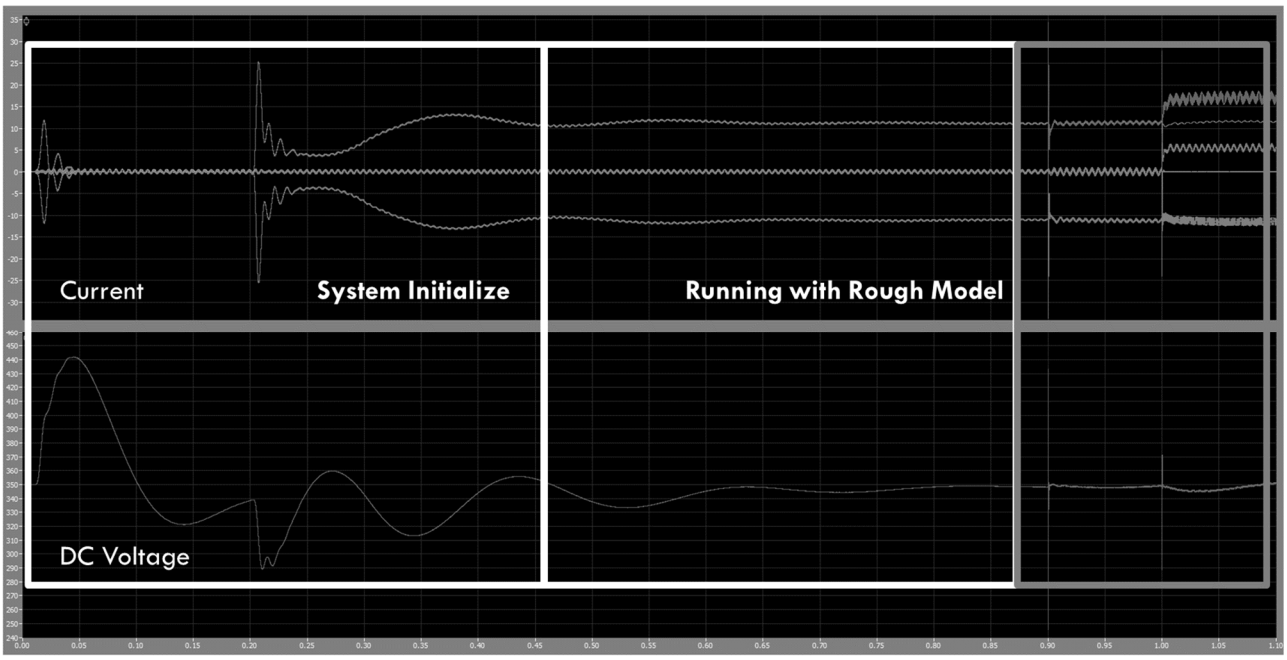

Figure 4-1 The Total Process of Simulation with a Single Ground Fault Happens

Before doing transient analysis, it is imperative to have an overlook of the whole process of the DC microgrid system as it is shown in Figure 4-1. There are two simulation result showing in this series of figures which have different fault locations. The whole simulation time (1.2s) can be divided into four major parts: the system initialization, operation with rough model, operation with detailed model, fault happen and after fault happen. Currents and DC voltage are shown in separate windows. In Figure 4-1 the first two highlight boxes correspond to the first two states. In first state, the system initializes with current and voltage changes violently due to the system components and loads are switching in gradually. In the second box, the system current and voltage become

stable with the rough cable model. Before the detailed model switching time, the system is under the normal operation as other non-cable research can reach too. The unique process starts here as the detailed cable model switches in and fault applies.

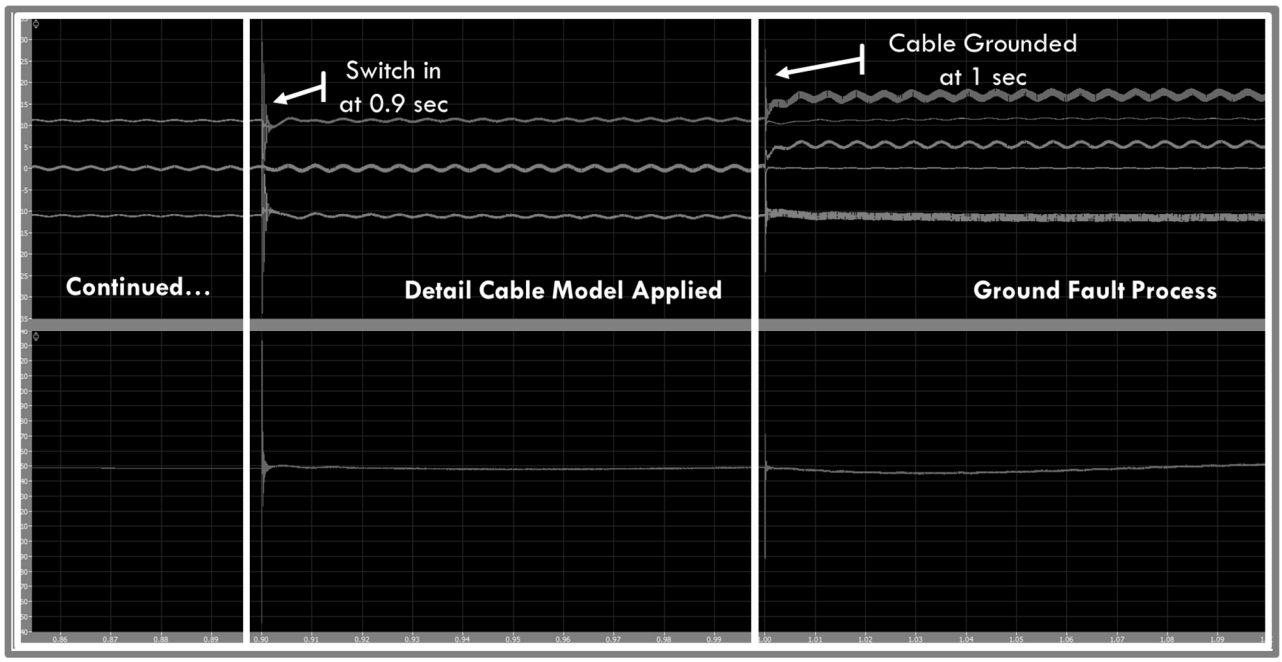

Figure 4-2 Voltage and Current during the Detailed Model and Fault Happens

The remaining two state can be seen more clearly in the Figure 4-2, as it zooms in the third box of the Figure 4-1. This figure contains two important time nodes: the time (0.9s) that detailed cable model is switched in and the time (1.0s) that ground fault is applied to the cable. The current and voltage remains relatively stable except the two switching time points. There are surges during the two switching time nodes, which is because the charge and discharge process of new detailed model and the ground path created by the fault respectively. It should be noted the top current that levels up after fault indicates the current flowing through sending point the fault cable, and the middle current that levels up after fault indicates the CM current in the sending point of hub garages panel. Other current signals, including the receiving end of both current and the sending point current of normal cable, remains the same value level after fault.

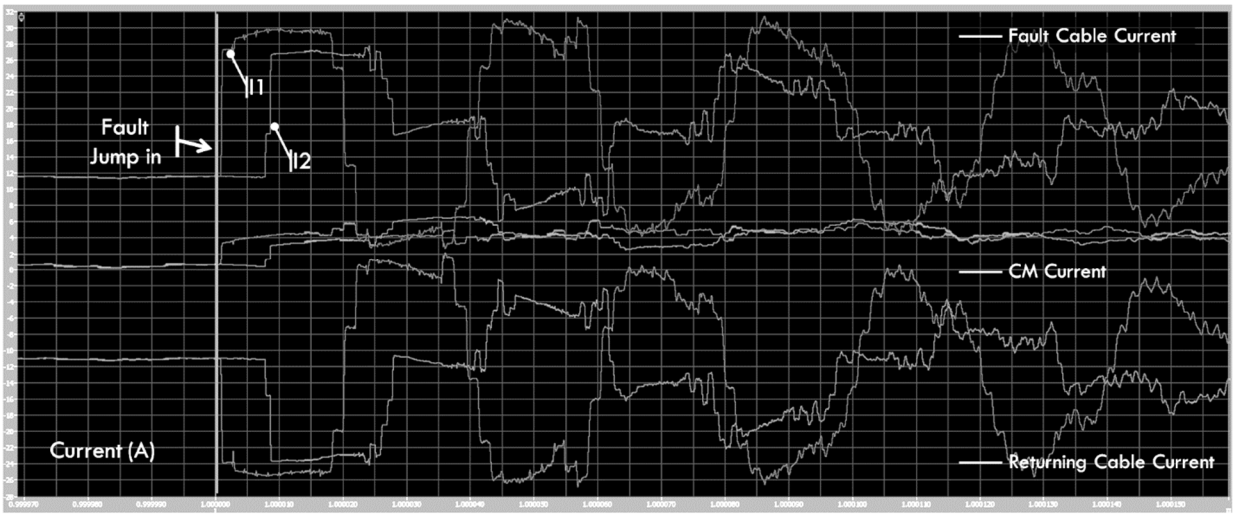

Figure 4-3 Zoom in View of Current of Cables

The zoom in vision gives us a better view to see the effect of traveling wave in the Figure 4-3. We can first note that there are two obvious currents in each current type regarding to the different fault location situation. With similar current appearance of pattern for both situation, the delay is easy to be observed. The delay is caused by the signal passing the different length before flowing into the ground, which we can use it as a basis to calculate the fault distance later. Other things we can see from this figure is the CM current does not have a good definition, which is because it's almost the same and contrary signal in the returning cable.

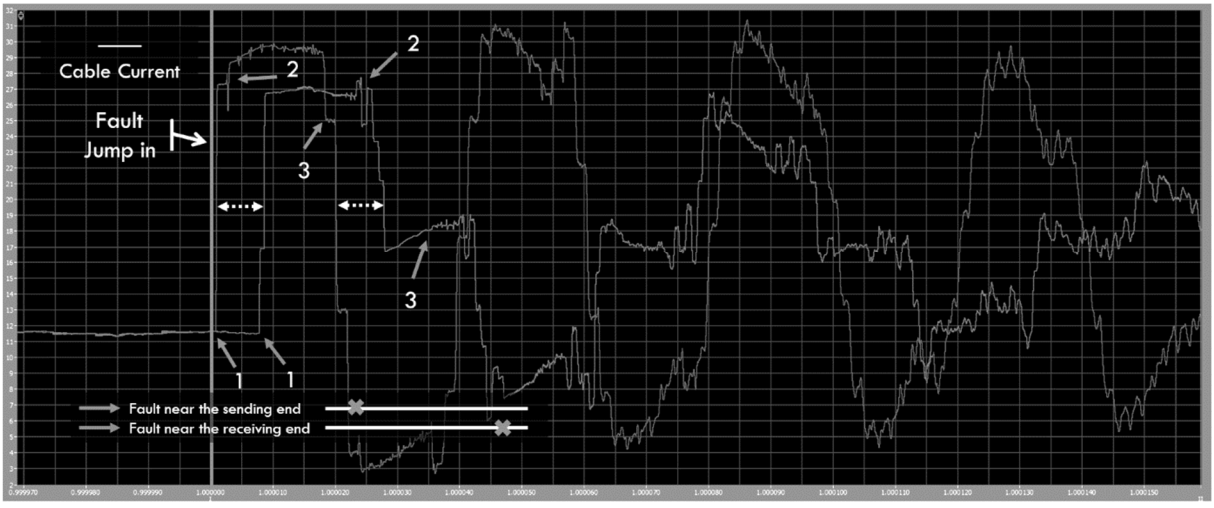

Figure 4-4 The Sending End Current of Fault Cable with Two Fault Location Situation

The sending point current of fault cable is selected to apply the further analysis with wavelet, which is presented in Figure 4-4. One of the situation is that the fault happens in the near sending end, while the other situation is that the fault happens in the near receiving end. The pair of arrows with same number point to the same turning point that in both situations. For the same turning point, the delays and the distance between turning points are almost the same. It is impossible to achieve two different fault location situations in the reality for location, but the constant time difference between certain turning points can help us. This tells that we can calculate and verify the correctness of data if we can catch these turning point of currents with limited error.

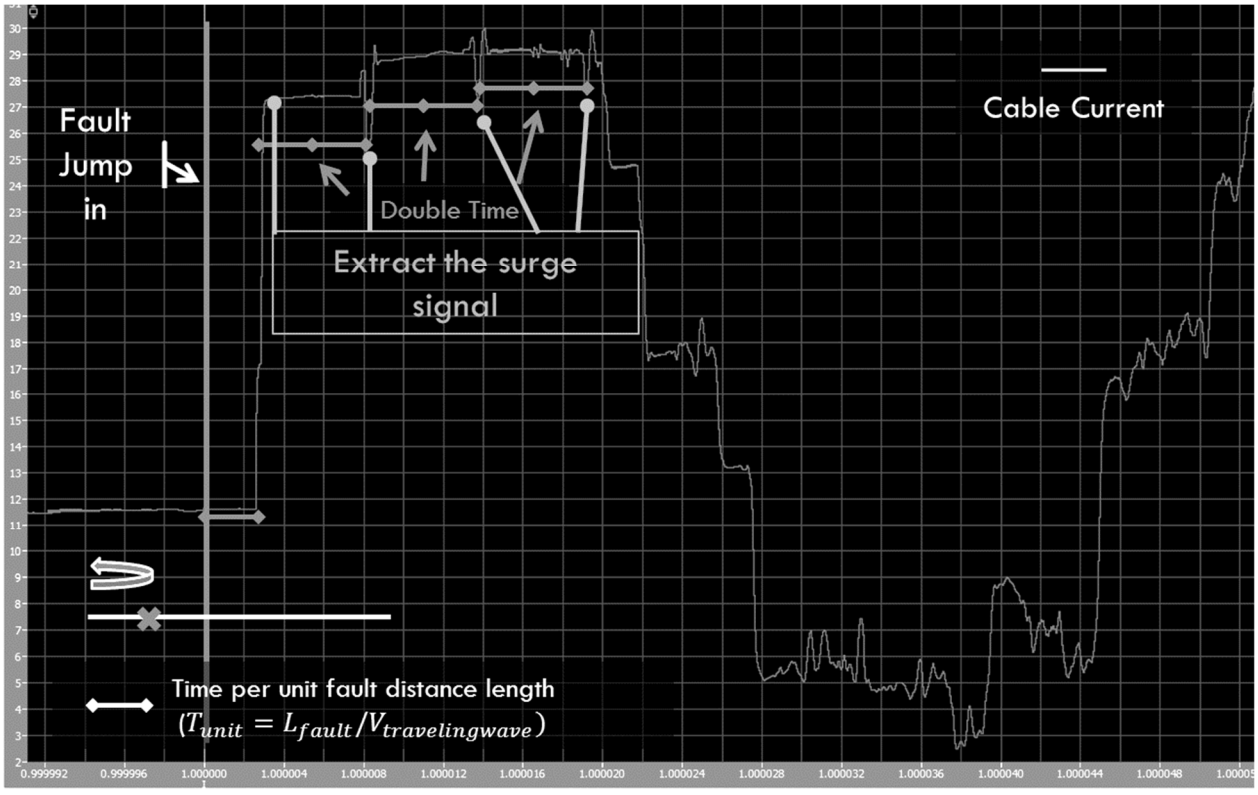

Figure 4-5 Calculation of Distance Using Traveling Wave Theory

We can derive the algorithm that how to calculates the distance of the fault. As the positive surge will reflect at the fault point and go back to the sending point as a negative current, it generates a negative surge at the sending point. The time is just as the same as the wave go forward and back between the sending point and fault point shown in Figure 4-5. So we have

$$T_{points} = 2 \times L_{fault} / V_{travelingwave} \quad \text{Equation 4-1}$$

The key, is to extract the surge signal, as well as we called the turning point previously. Then we can use it to calculate the distance by applying the Equation 4-1.

4.2.2 Applying the Wavelet Packet

As it is the most important part to achieve the traveling wave method, how to extract the surge signal becomes crucial. This is the place that needs wavelet packet.

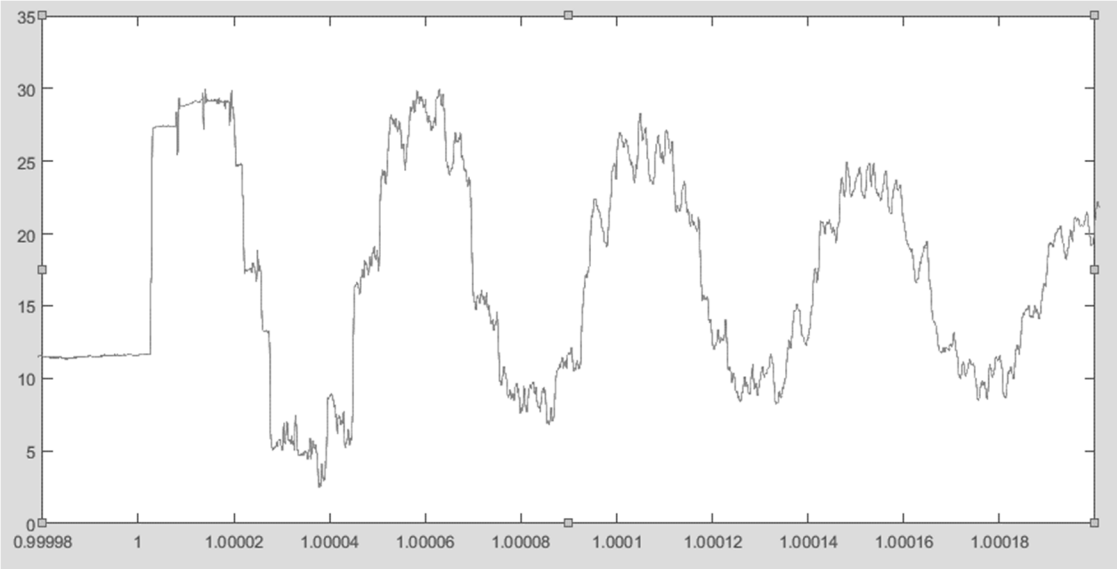

Figure 4-6 Original Data Display in MATLAB

The original signal is shown in the figure 4-6 as an example. The signal length is $2ms$, as the sampling time is $50ns$, which will result in 40000 data points in every sample. This is the data parameters of the root node in the wavelet tree.

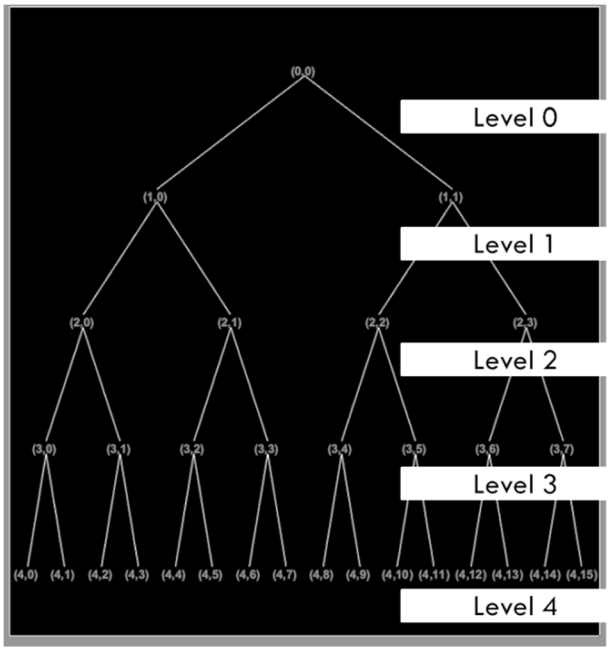

Figure 4-7 Wavelet Packet Decomposition Tree

Figure 4-7 shows the wavelet packet decomposition tree. In this model, we use the Db5 mother wavelet to reach a balance point of computing speed and clear boundary between frequency bands, which is discussed later. The level of decomposition is set to be 4 as the data contains valuable information can be get from some nodes of the level.

Table 4-2 Wavelet Tree Information

Level	Data Per Node	Time Interval	Relative Resolution
0	40000	0.05 μs	*1*
1	20000	0.1 μs	1/2
2	10000	0.2 μs	1/4
3	5000	0.4 μs	1/8
4	2500	0.8 μs	1/16

Table 4-2 shows the data points, time interval and relative resolution in every node of different level in wavelet decomposition. The *level 0* represents the original data as the root node (0,0). It can be seen as the level goes deeper, the data are cut half by half. The time interval, which represents the absolute resolution enlarged with the relative resolution decreasing. As the traveling speed is extremely fast, if we lose a lot time resolution, it may cause unexpected error in the result. The appropriate level for further data extracting should be carefully considered.

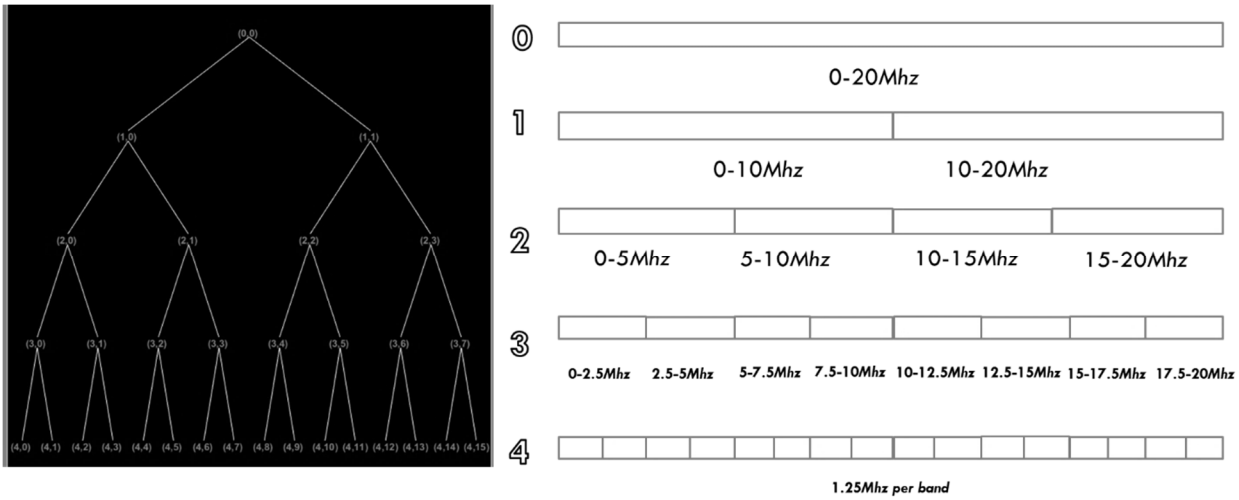

Figure 4-8 The Wavelet Packet Tree and its Corresponding Frequency Bands

Using wavelet packet, the adequate frequency band selection is as important as selecting the decomposition layer. Figure 4-8 shows the frequency distribution by the wavelet packet decomposition under the setting previously. As narrower band get, the more possibility exists to fetch a signal with less unwanted components that not contain the information of surge signals. But as the resolution becomes bad as the frequency bands get narrower. A balanced selection of frequency band should be made. In this case, the 2.5Mhz frequency band, which corresponds to decomposition level 3, will be the last layer in the analysis. Next step is to get the most suitable frequency band in decomposition process.

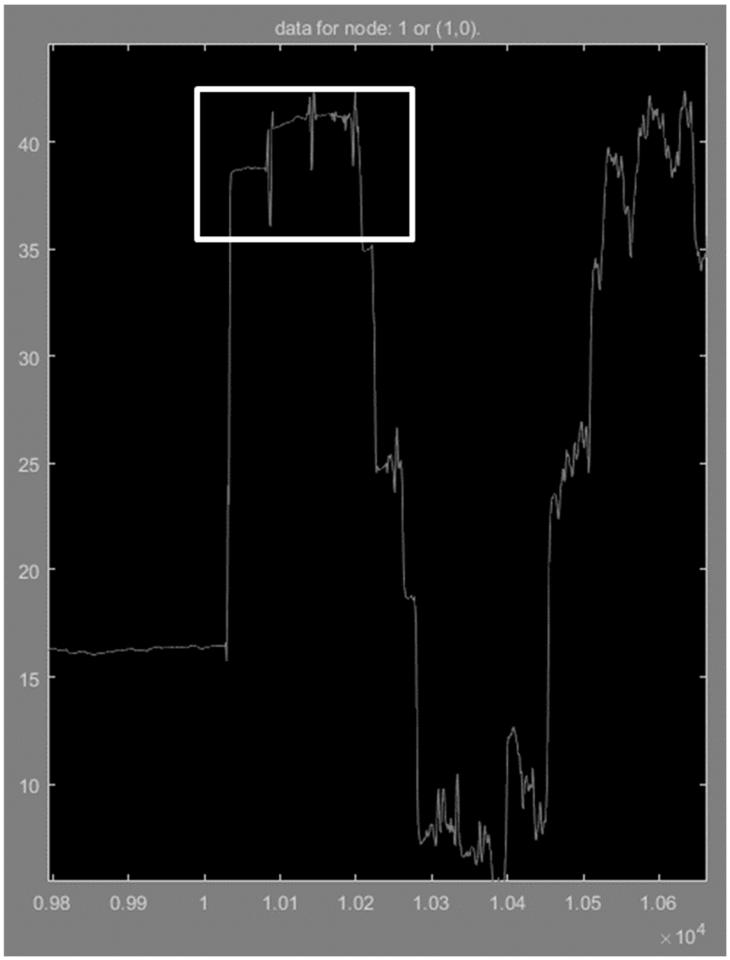

Figure 4-9 Wavelet Packet Decomposition Node (1,0)

The Figure 4-9 shows the wavelet packet decomposition node (1,0), which corresponds to the frequency band 0 – 10Mhz. The three surge signals remain obvious as the white box points out. This means the fault information for traveling analysis is still ambient in the frequency band. In the other hand, in 10Mhz – 20Mhz frequency band, noises are too much, even covering the valuable information, which cannot be used.

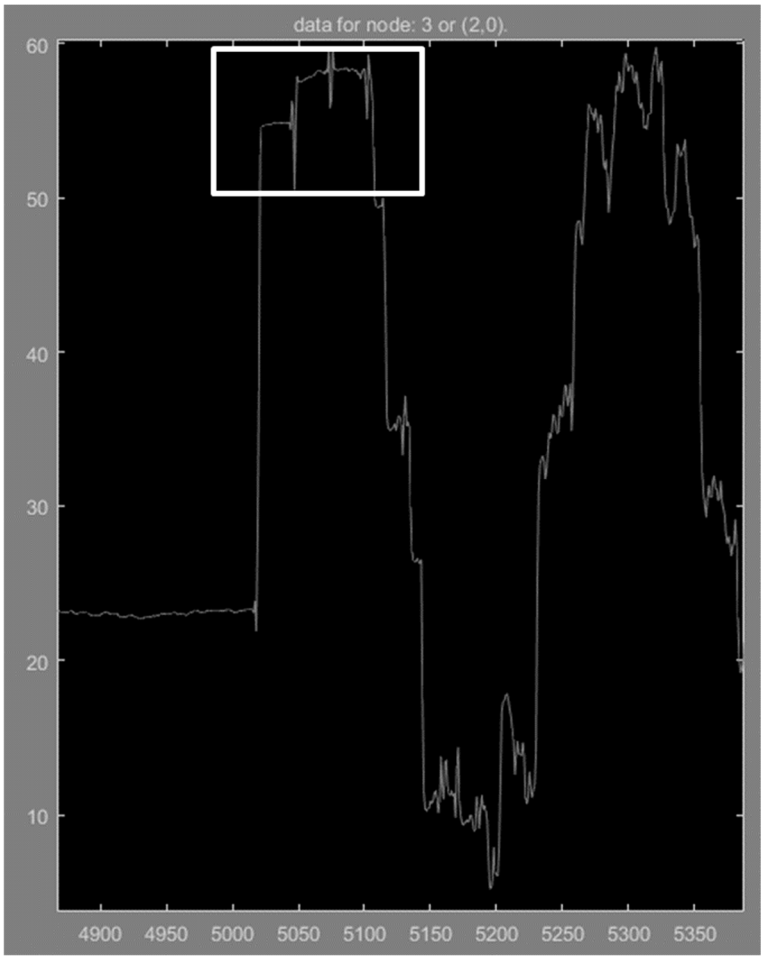

Figure 4-10 Wavelet Packet Decomposition Node (2,0)

The Figure 4-10 shows the wavelet packet decomposition node (2,0), which corresponds to the frequency band 0 – 5Mhz. Similar like analysis previously, the signals in the white box still exists, meaning information remains enough to be extracted in further analysis. Actually, the surge single already contains some component in the frequency band between 5 – 10Mhz, but the amplitude is not satisfied for an accurate location. The main part remains in the lower frequency band in this level.

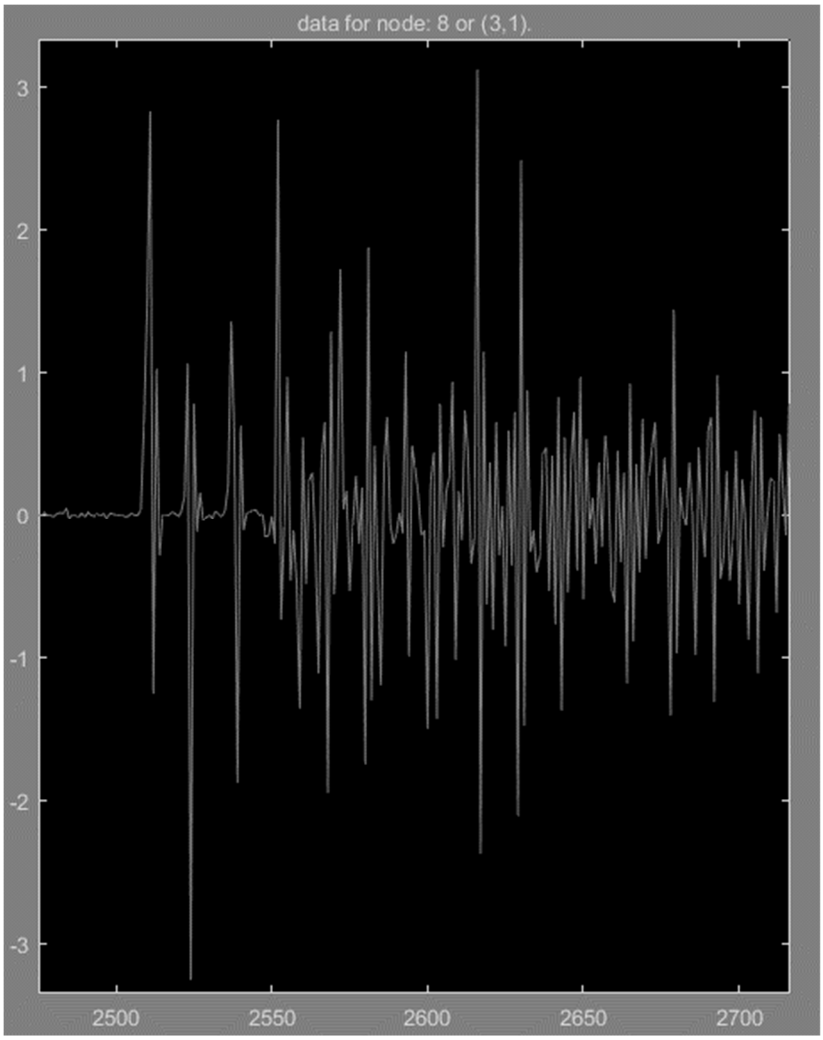

Figure 4-11 Wavelet Packet Decomposition Node (3,1)

The Figure 4-11 shows the wavelet packet decomposition node (3,1), which corresponds to the frequency band 2.5 – 5Mhz. Unlike previous two decomposition step, in this step the higher frequency band is selected to be ready for final analysis later. The reason that we use the frequency band is this frequency band already contains enough location fault information as the resolution is also appropriate regarding to the length of the cable. On the other hand, in frequency band 0 – 2.5Mhz, the edge of surge signals become not sharp as the high frequency components not exists anymore, which is not good for fault location. The analysis is implemented using the node (3,1) to calculate the fault location.

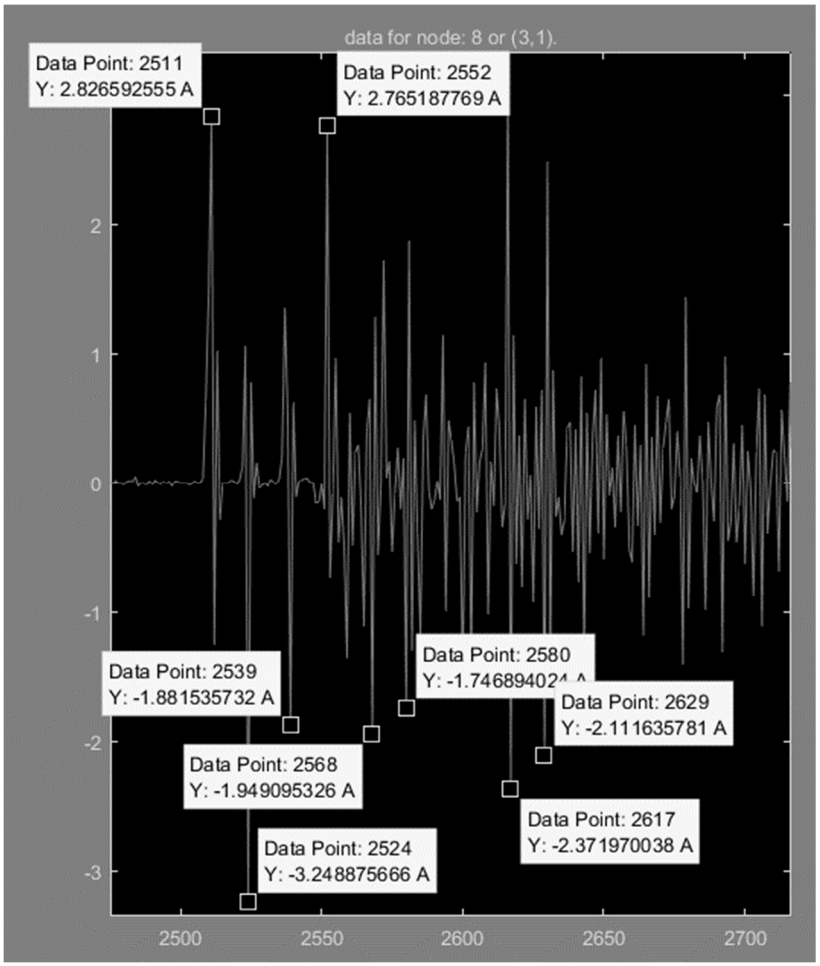

Figure 4-12 Fault Location Algorithm Approaching in Node (3,1)

The fault location algorithm is implemented by using the data in Node (3,1). Four steps can be used to get the fault location distance (from the sending point) of the cable:

1 Mark the peak values (negative first) (Shown in Figure 4-12)

2 Calculate distance between the marked points $\Delta Point_{data}$

$$\Delta Point_{data} = P_{d1} - P_{d2} \quad \text{Equation 4-2}$$

3 Calculate the time interval $\Delta Time_{data}$

$$\Delta Time_{data} = \Delta Point_{data} \times Time_{point} \quad \text{Equation 4-3}$$

4 Calculate the fault distance by multiplying the wave speed to the average time interval and then divide by 2

$$L_{fault} = \Delta Time_{data\_avg} \times \frac{V_{cable}}{2}$$ Equation 4-4

In this case, 8 peak values are marked. The difference of data point $\Delta Point_{data} = 12{,}13$. So the time interval $\Delta Time_{data} = \Delta Point_{data} \times 0.4\ \mu s \cong (4.8 - 5.2)\ \mu s$. And the distance can be calculated as

$$L_{fault} = 5\mu s \times \frac{V_{cable}}{2} = 120\ m$$

Where the $V_{cable} = 5.4 \times 10^7\ m/s$ is calculated from the cable parameters in the Table 4-1.

The simulation fault happens at the distance 124m. So the error rate is

$$\frac{124 - 120}{124} \times 100\% \cong 3.23\%$$

That proves this method can be used in the fault location of cables.

4.2.3 Result Analysis and Discussion

Table 4-3 Result Analysis of Traveling Wave Method

No.	Fault Location Simulated (m)	Calculated Location (m)	Error Rate (%)
1	41	45	9.7
2	83	87	4.8
3	124	120	3.23
4	166	163	1.8
5	212	207	2.4
6	264	269	1.9
7	290	287	1.0
8	331	326	1.5
9	370	365	1.3

We have applied 9 different fault location situations into the simulation and the results are shown in the Table 4-3, with same algorithm used in the example below. As the distance gets closer to the sending end, the result tends to be more inaccurate. This shows the difficulty will be heavier when the fault happens near the sending point of cable.

The fault impedance as well as ground resistance will have some impact to the detection. But as the inductance in the fault point is relative small when the short is developed totally, the result accuracy will not be influenced in certain degree. The resistance in the ground fault path will not disturb the traveling wave appearance. But when high resistance grounding exists in other cables fault scenario, the amplitude will be as tiny as other interference may act similar. That will become hard to extract the useful signals.

4.3 Stable Parameter Analysis

Stable Parameter Analysis focuses the stable current while the system continues to operate with the fault remaining. It is seen as an online detection way as no more injection and more exterior measuring devices should be used. Stable parameter analysis can be a complimentary method for other method.

4.3.1 CM Current

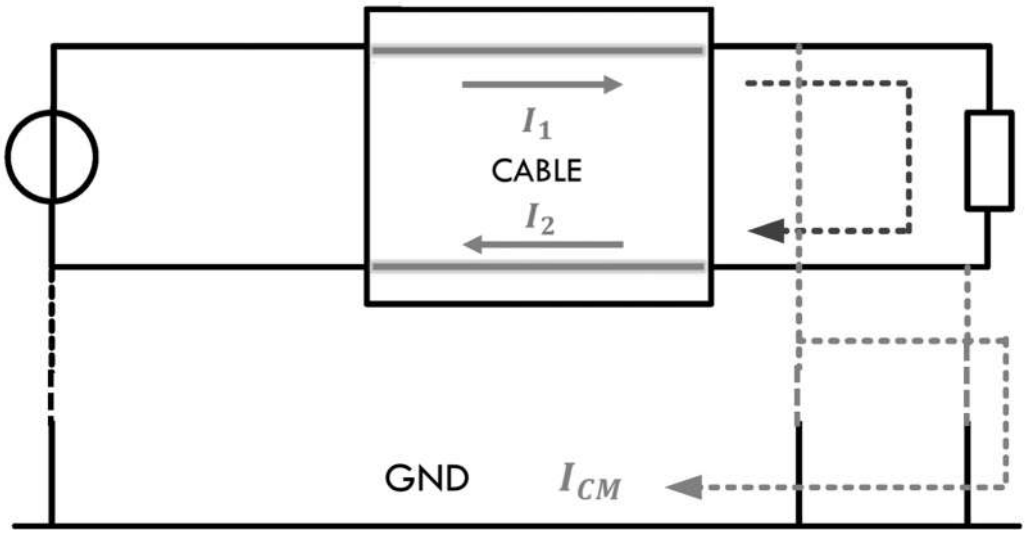

Figure 4-13 CM Current in Cable system

Common Mode (CM) current, is a useful tool when the system encounter problems with the ground. The definition of CM current, shown in Figure 4-13 can be described as

$$I_{CM} = \frac{I_1+I_2}{2} \qquad \text{Equation 4-5}$$

In normal operation, the current flow through forward and back cable should be exactly the same if assuming they are grounded in the same situation by capacitor. So the common current I_{CM} just contains the ground current from the Figure 4-13 structure. When the ground fault happens, the ground current will change suddenly as the cable fault between the hub and participating garage

should appear obviously in its current values. As the supply of the loads are maintained while the fault exists, the cable can still feed the garage and house for a while. This will happen in the DC community grid since the fault current will not be large to threaten the overall grid operation.

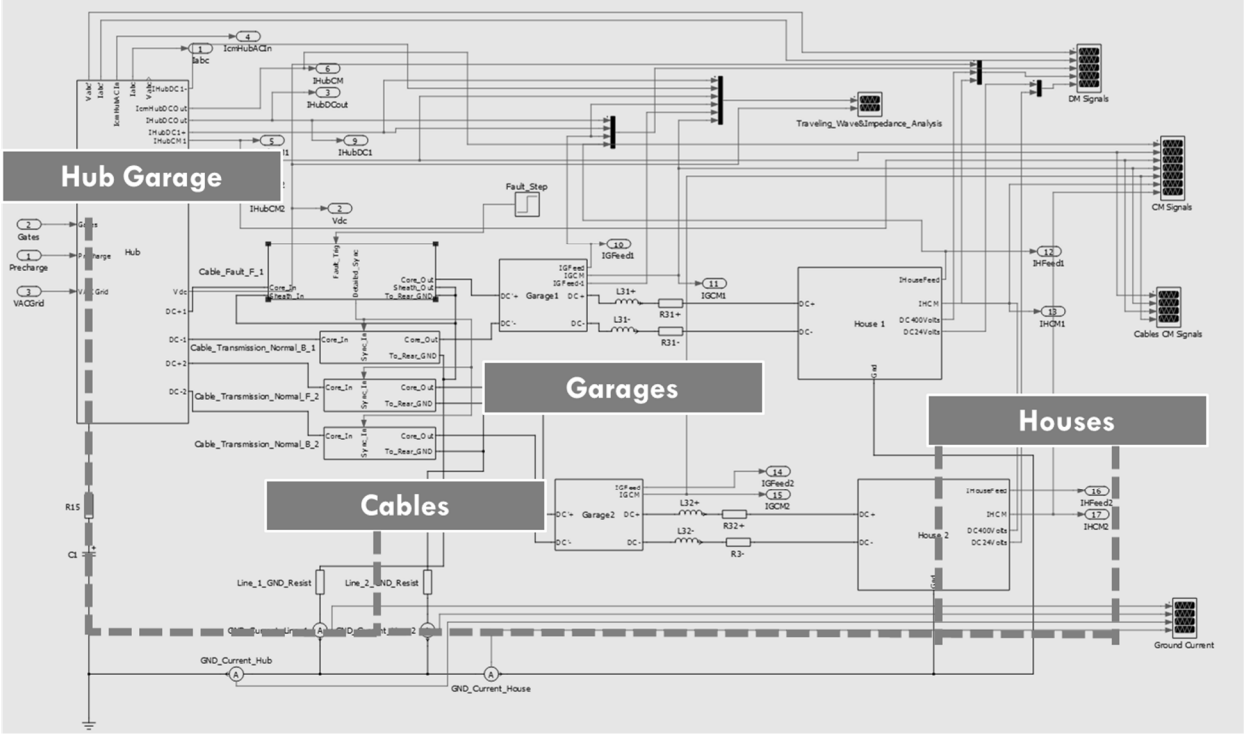

Figure 4-14 The Ground Fault Current Paths in the Model

The Figure 4-14 shows the possible paths for the ground fault current to flow through. It should be noted that the participating garages are not connected to the ground. Compared to the path connected between the hub garage and fault cable, the path between houses and fault cable appear as high impedance circuit. In this model, the main current after fault happens will flow through the fault point to the hub garage.

4.3.2 Stable CM Current Simulation Result and Analysis

By setting different fault location and measuring the CM current in the sending end of pair of cables which one of them has fault, we can get the CM current values. The simulation model and parameters setting are the same as the model in traveling wave analysis section.

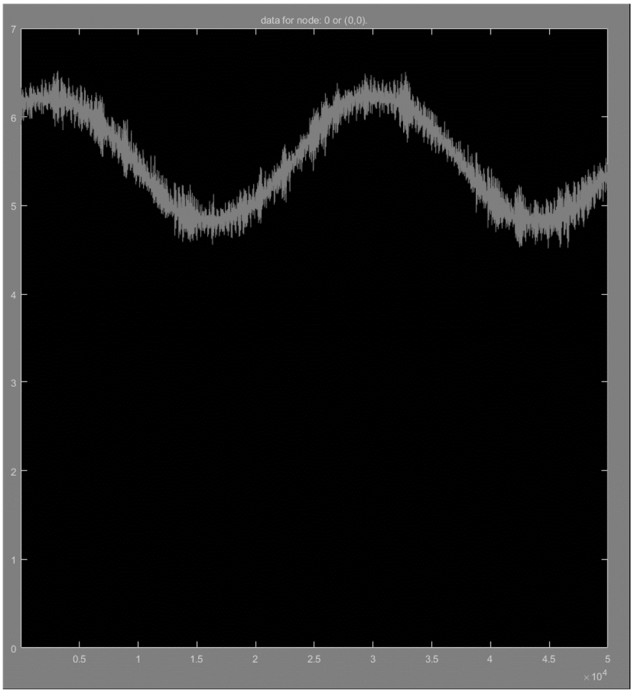

Figure 4-15 Original Signal in Stable System After Fault

From the Figure 4-15 we can see the original signal contains high frequency components and small peaks that may influence the measurement. Since the stable parameter does not need high sample frequency devices, it is more possible the measurement device gets the artificial accident signal that leads to improper warning or action. Wavelet can help decrease this possibility with no more filter hardware.

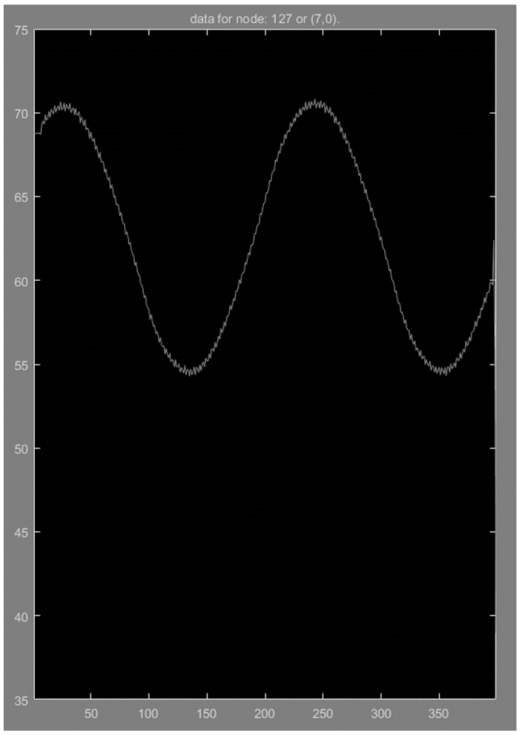

Figure 4-16 Processed Signal by Wavelet

Figure 4-16 present the signal after wavelet process where all the high frequency components are eliminated. It should be noted we select the lowest frequency band to get the smooth curve instead of the image in traveling wave analysis. There is no peak signal we want to extract, so the selection of frequency band is different.

All the CM current data are processed by the wavelet packet and the further analysis can be continued.

Table 4-4 Stable CM Current After Fault

No.	Distance from Sending End (m)	Current (A)
1	41	5.7108
2	83	5.6823
3	124	5.6572
4	166	5.6241
5	212	5.6031
6	264	5.5784
7	290	5.5510
8	331	5.2492
9	370	5.4990

Table 4-4 shows the CM current when the system steps into stable after fault triggered. The ground resistance in this case is set to 20 Ohms. It can be seen that a good liner characteristic is shown for this series of current values. As the system is in stable operation, the difference of inductance in the cable will not influence the DC current flowing the ground. The main reason that cause the current to differ from each other comes from the resistance of the fault part in the cable.

This method will be influenced by the different parameters of outside circuits. The ratio of cable resistance and outside resistance will decide whether the method can be successfully achieved. If the outside resistance is much higher than the cable resistance, this method may will not work well. In addition, the ground current value also sensitive to the environment which will cause the change of ground resistance.

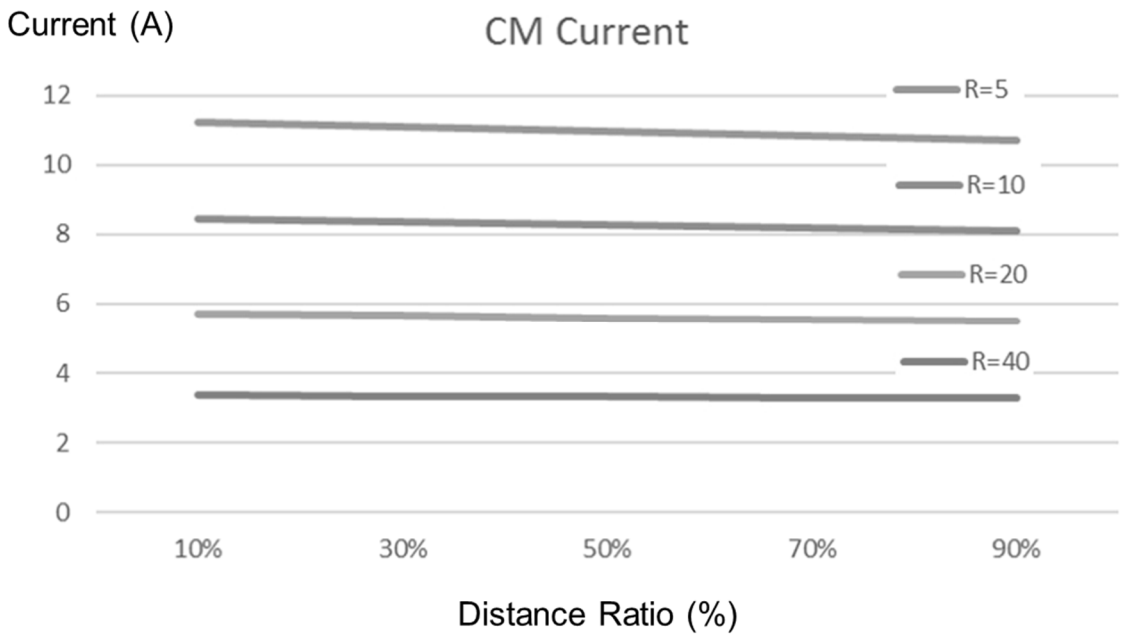

Figure 4-17 CM Current under Different Ground Resistance

This can be easily shown from the Figure 4-17 that the different ground resistance can lead to huge changes of the CM current values. Although all the results are liner with the distance ratio change, it's hard to find the absolute distance when this method takes into real application.

4.3.3 Reference Signal for CM Current Fault Location Method

In order to find the absolute fault location using the stable parameter method, references signal must be found to be established the equivalent circuit outside the cable model. This signal should reflect the characteristic of the system in the normal operation to help the location of fault.

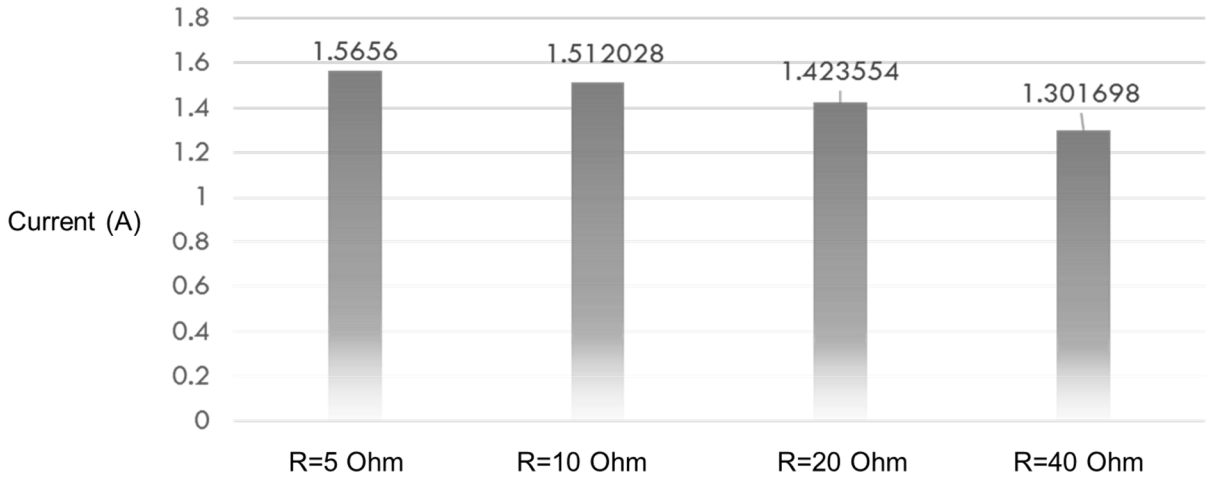

Figure 4-18 CM Peak-Peak Current Value Before Fault

CM peak-peak current can be selected as a potential factor to decide the outside circuit as shown in Figure 4-18. The CM peak-peak current is coming from the leaking current flowing through the capacitors. There are different for different ground resistance situation, which we can use to put more analysis to set a connection between the normal operation parameters and the parameters when the fault happens.

4.4 Summary

Two major methods are applied for this DC community microgrid model in this chapter. As the traveling wave will have more advantage preventing from the outside parameter changes, it will need a high frequency sensor and its facility equipment since the traveling wave speed is extremely high and the transient process is short. The stable parameter analysis overcome these disadvantages, but it is subject to the outside circuit and environment. A careful connection between reference signal and fault signal should be connected with huge data collected.

Chapter 5 Conclusion and Future Work

The conclusion and future work are shown in this chapter.

5.1 Conclusion

For DC community microgrid, new fault detection and location system needs to be developed as the microgrid contains different features compared to AC grid. As key components in the microgrid, the cables provide the connection between every participating unit. It is necessary to develop fault detection and location system to help find and fix the fault happens inside the cable. Single ground fault is one type of common fault as the cable being damaged by exterior force. Traveling wave and stable parameter analysis can be used to locate the ground fault in a relatively long cable.

The signal may contain irrelevant components, and wavelet packet can help filter them out. For traveling wave method, wavelet can help extract the certain signals to determine the traveling time interval for calculation the fault distance; For stable parameter analysis, wavelet packet can perform as an online low pass filter protect the current sensor from sudden fake signals.

5.2 Future Work

Both method mentioned in this thesis have disadvantages and these block them from implementation in the reality.

The reason why external signal becomes popular method is that it can directly or indirectly generate significant fault signals. For traveling wave method, the high definition and better data filter and recognition technic should be developed. Or the way to lower down the requirement of high sample rate sensor can be considered. For stable parameter analysis, the key is to find reasonable and accurate expression of the outside circuit of cables. With this problem solved, the

analysis will be much easier using simple equivalent model to represent the whole DC microgrid system.

As the smart diagnose develops fast in a lot of industrial area, the fault detection and location of cables will follow the same trend as the cloud, big data, neural network being introduced. The ultimate goal is to use already devices monitoring the cables to achieve the location instead of using external equipment, which is more economic and intelligent.

References

[1] N. Hatziargyriou, H. Asano, R. Iravani, and C. Marnay, "Microgrids," *IEEE Power and Energy Magazine,* vol. 5, pp. 78-94, 2007.

[2] C. Alvial-Palavicino, N. Garrido-Echeverria, G. Jimenez-Estevez, L. Reyes, and R. Palma-Behnke, "A methodology for community engagement in the introduction of renewable based smart microgrid," *ENERGY FOR SUSTAINABLE DEVELOPMENT,* vol. 15, pp. 314-323, 2011.

[3] R. H. Lasseter and P. Paigi, "Microgrid: a conceptual solution,", 2004, pp. 4285-4290 Vol.6.

[4] X. Liu, P. Wang and P. Loh, "A Hybrid AC/DC Microgrid and Its Coordination Control," *IEEE TRANSACTIONS ON SMART GRID,* vol. 2, pp. 278-286, 2011.

[5] M. Jianmei, W. Li and H. Suyang, "Research on online detection and location of multi-conductor cables' faults,", 2016, pp. 1-5.

[6] A. Pinomaa, J. Ahola, A. Kosonen, and T. Ahonen, "Diagnostics of low-voltage power cables by using broadband impedance spectroscopy,", 2015, pp. 1-10.

[7] J. Yang, J. E. Fletcher and J. O'Reilly, "Short-Circuit and Ground Fault Analyses and Location in VSC-Based DC Network Cables," *IEEE Transactions on Industrial Electronics,* vol. 59, pp. 3827-3837, 2012.

[8] X. Yang, M. S. Choi, S. J. Lee, C. W. Ten, and S. I. Lim, "Fault Location for Underground Power Cable Using Distributed Parameter Approach," *IEEE Transactions on Power Systems,* vol. 23, pp. 1809-1816, 2008.

[9] J. Zhai, Y. Ding, B. Xu, and Y. Li, "Wavelet and travelling wave based DC cable fault localization in MTDC,", 2012, pp. 206-209.

[10] R. Meyur, D. Pal, N. A. Sundaravaradan, P. Rajaraman, K. V. V. S. Srinivas, M. J. B. Reddy,

and D. K. Mohanta, "A wavelet-adaptive network based fuzzy inference system for location of faults in parallel transmission lines,", 2016, pp. 1-6.

[11] M. Shafiullah, M. Ijaz, M. A. Abido, and Z. Al-Hamouz, "Optimized support vector machine & wavelet transform for distribution grid fault location,", 2017, pp. 77-82.

[12] Q. Shi and O. Kanoun, "Detection and location of single cable fault by impedance spectroscopy,", 2014, pp. 595-599.

[13] M. Lattner, W. Carr and C. Benner, "Improved fault location on distribution circuits using advanced inputs,", 2016, pp. 1-8.

[14] J. Zhang, W. Chu, Q. Yao, J. Zhou, and Z. Bo, "The design based on mathematical morphology and wavelet theory of fault location system on power cables,", 2011, pp. 1521-1524.

[15] A. Wang, M. Zhang, H. Xu, and Y. Wang, "Location of Wire Faults Using Chaotic Signal," *IEEE Electron Device Letters,* vol. 32, pp. 372-374, 2011.

[16] T. Zhihai, G. Liang, K. Taileng, Z. Fengqing, Z. Yu, H. Xiaoyun, P. Feijin, and L. Xiang, "An accurate fault location method of smart distribution network,", 2014, pp. 916-920.

[17] M. Wang and T. Stathaki, "Online fault recognition of electric power cable in coal mine based on the minimum risk neural network," *Journal of Coal Science and Engineering (China),* vol. 14, pp. 492-496, 2008-01-01 2008.

[18] J. Livie, P. Gale and A. Wag, "The Application of On-Line Travelling Wave Techniques in the Location of Intermittent Faults on low Voltage Underground Cables,", 2008, pp. 714-719.

[19] E. C. Bascom, D. W. Von Dollen and H. W. Ng, "Computerized underground cable fault location expertise,", 1994, pp. 376-382.

[20] G. Thomas, A. Emadi, J. Mijares-Chan, and D. A. Buchanan, "Low frequency ultrasound NDT of power cable insulation,", 2014, pp. 1126-1129.

[21] A. K. Pradhan and R. Mohanty, "Cable fault location in a DC microgrid using current injection technique,", 2016, pp. 1-6.

[22] M. C. R., P. K. and J. S. Z., "System specification for a DC community microgrid and living laboratory embedded in an urban environment," in *2015 International Conference on Renewable Energy Research and Applications (ICRERA)*, 2015, pp. 1119-1125.

[23] W. A. Thue, *Electrical Power Cable Engineering, Third Edition*: CRC Press, 2016.

[24] F. P. A. National, *NFPA 70 National Electrical Code 2014*: National Fire Protection Assn, 2013.

[25] Z. Haibo, F. Gruson, D. Florez, and C. Saudemont, "Analysis of the influence of different cable modelling for DC series offshore wind farm,", 2016, pp. 1-9.

[26] J. G. Proakis and D. G. Manolakis, *Digital Signal Processing*: Pearson Prentice Hall, 2007.

[27] K. Gröchenig, *Foundations of Time-Frequency Analysis*: Birkhäuser Boston, 2013.

[28] I. Daubechies, "The wavelet transform, time-frequency localization and signal analysis," *IEEE Transactions on Information Theory,* vol. 36, pp. 961-1005, 1990.

[29] L. Debnath, *Wavelet Transforms and Time-Frequency Signal Analysis*: Birkhäuser Boston, 2001.

[30] N. Hess-Nielsen and M. V. Wickerhauser, "Wavelets and time-frequency analysis," *Proceedings of the IEEE,* vol. 84, pp. 523-540, 1996.